WORKING PAPER

Mapping global tropical wetlands from earth observing satellite imagery

Thomas Gumbricht

CIFOR

Working Paper 103

Mapping global tropical wetlands from earth observing satellite imagery

Thomas Gumbricht

Working Paper 103

Gumbricht, T. 2012 Mapping global tropical wetlands from earth observing satellite imagery. Working Paper 103. CIFOR, Bogor, Indonesia.

Cover photo by Yves Laumonier/CIFOR
A view of swamp forest in Danau Sentarum National Park, Tekenang hill, Kapuas Hulu, West Kalimantan, Indonesia.

CIFOR
Jl. CIFOR, Situ Gede
Bogor Barat 16115
Indonesia

T +62 (251) 8622-622
F +62 (251) 8622-100
E cifor@cgiar.org

cifor.org

Table of contents

List of figures and tables

Figures

Tables

Abbreviations

BRDF	Bidirectional reflectance distribution function
CIAT	*Centro Internacional de Agricultura Tropical* (International Center for Tropical Agriculture)
DCW	Digital Chart of the World
DEM	Digital elevation model
ENVISAT	Environmental satellite
EOS	Earth observing satellite
EROS	Earth Resources Observation and Science
ESA	European Space Agency
ET	Evapotranspiration
EWDI	Enhanced wetness difference image
GTI	Global topographic index
GTWI	Global topographic wetness index
HWSD	Harmonized World Soil Database
IIASA	International Institute for Applied Systems Analysis
ITCZ	Inter-tropical Convergence Zone
JAXA	Japanese Aerospace Exploration Agency
JRC	Joint Research Council
K&C	Kyoto and carbon
LSWI	Land surface water index
MERIS	Medium resolution imaging spectrometer
MFD	Multiple flow direction
MIR	Mid-infrared
MODIS	Moderate resolution imaging spectroradiometer
NDPI	Normalised difference pond index
NDVI	Normalised difference vegetation index
NDWI	Normalised difference wetness index
NIR	Near-infrared
PALSAR	Phased array type L-band synthetic aperture radar
PBI	Perpendicular background index
PBWI	Perpendicular background wetness indicator
PCA	Principal component analysis
PVI	Perpendicular vegetation index
PWI	Perpendicular wetness index
SAM	Spectral angle mapper
SAVI	Soil adjusted vegetation index
SFD	Single flow direction
SRTM	Shuttle Radar Topography Mission
SWIR	Short-wavelength infrared region
TC	Tasseled cap
TM	Thematic mapper
TPI	Topographic position index
VIS	Visible (usually red) wavelength
WDVI	Weighted difference vegetation index

Acknowledgments

The MODIS data were obtained through the online Data Pool at the NASA Land Processes Distributed Active Archive Center (LP DAAC), USGS/Earth Resources Observation and Science (EROS) Center, Sioux Falls, South Dakota (https://lpdaac.usgs.gov/get_data).

This work is supported by the United States Agency for International Development (USAID) through grant No. EEM-G-00-04-00010-0O.

Summary

Wetlands have a high biodiversity, and are key regulators of the flow of water and the fluxes of mineral and nutrients from land to sea. Wetlands only cover a few percent of the global land surface, but their soils contain as much carbon as the entire biosphere. Yet the extent, volume and carbon content of the world's wetlands are not accurately known, in particular, for tropical and sub-tropical regions. Despite their importance, wetlands have historically been regarded as wastelands, and have largely been ignored in studies of climate change. Improved maps of the distribution of global tropical wetlands, their volumes and carbon contents are urgently needed. Because wetlands are characterised by their water, soil and vegetation conditions, they are difficult to identify from satellite images of earth. Few of the existing efforts at mapping the global land surface have attempted to identify wetlands.

Wetlands exclusively occur under certain topographic conditions, and where the soil and water conditions are such that inundation can, and actually does, occur on a regular (annual) basis. Taking this as a starting point, a set of novel indexes relating to wetlands was developed. The first index is a climatic topographic wetness index. Using a global digital elevation model, combined with global climate data, a tropical global map of surface wetness was created. Using global optical satellite images from the moderate resolution imaging spectroradiometer (MODIS) a second wetness index was developed. Compared to previous satellite-based wetness indexes, the index attempts to remove the vegetation influence and focus on the soil surface wetness. From an annual time-series of MODIS images, the inundation cycle of the global tropics was captured. The two wetness indexes are strong candidates for mapping the distribution of global tropical wetlands.

Traditional image classification is based on reference data, and usually attempts to delineate features from a single image. As wetlands are characterised by annual variations in inundation, an approach for classifying wetlands from a chrono-sequence of annual MODIS images was developed. In the chrono-sequence, only locations with similar climatic seasonality, and within spatial proximity were classified based on a reference site. Wetlands, often with vegetation and wetness phenology out of phase compared to adjacent dry lands, can thus be delineated.

Initial results are promising for all approaches developed in this study; however, lack of reference sites and reference data has hitherto prevented the development of a global tropical wetland map.

1. Introduction

Wetlands are hotspots of biological diversity, productivity and reproduction. They are key regulators of water flow and biogeochemical cycles, including that of carbon. They control the flow of nutrients and pollutants from land to sea and protect the land from erosion. Wetlands are of interest to many scientific disciplines and are widely defined as 'lands transitional between terrestrial and aquatic systems where the water table is usually at or near the surface or the land is covered by shallow water' (Cowardin *et al.* 1979).

Wetlands can contain peat, the accumulated remains of organic tissue. Peat forms where anaerobic conditions, resulting from water inundation, suppress the decomposition of dead organic matter. Peat can form in most climatic zones; in tropical climates as mangrove and peat swamp forests, in sub-tropical and temperate climates as reed/sedge peat and forest peat, and as moss peat in boreal, subarctic and arctic regions.

The definition of peat relates to the amount (per cent of dry mass) of dead organic matter (or organic carbon) making up the soil. The actual per cent varies, but 30% organic matter is widely used as a threshold for defining peat. Peatlands are defined as areas with a naturally accumulated top (or near top) layer of peat. The minimum depth of peat for an area to qualify as peatland varies between at least 20 and 70 cm according to the discipline and region (Montanarella *et al.* 2006), but commonly is around 30 cm. For instance, Joosten and Clarke 2002 define peat as "sedentarily accumulated material consisting of at least 30% (dry mass) of dead organic matter", and peatland as "an area, with or without vegetation, with a naturally accumulated peat layer at the surface".

Bogs are ombrotrophic (ombrogenic) peatlands that rely solely on precipitation, whereas fens are minerotrophic peatlands fed by groundwater inflow and upstream nutrient supply. In regions with high precipitation, ombrotrophic peatlands dominate (e.g. in Indonesia and Malaysia). Peatlands in more arid regions, and away from the coast, are in general minerotrophic fens. Many wetlands receive water and nutrient inputs from both precipitation and groundwater flow, and even from fog (Price 1992). Riparian wetlands where peat might form can be seen as a special kind of fen.

In soil classification schemes, peat is classified differently in different regions and disciplines, but internationally peat is classified as histosol (FAO 1998). To qualify as a histosol the groundwater table must reach the peat (histic) surface for at least one month per year. The FAO (1998) classification includes more detailed definitions, and divisions into sub-classes.

Globally, peatlands cover approximately 3% of the land surface. They contain 550 gigatonne (Gt) of carbon, or about one-third of global soil carbon (Bain *et al.* 2011). Thus, the peat carbon stock equals the carbon stock in the total global biomass, and is double the carbon stock in world forests. The extent, volume and carbon content of the world's tropical peatlands are, however, not very accurately known. Page *et al.* (2011) estimate that tropical peatlands cover 441 025 km^2, an area which falls between earlier estimates of 275 000 to 571 000 km^2. More than half the world's tropical peat is found in South East Asia, where Indonesia has the lion's share. The same study estimates the total volume of tropical peat at 1758 cubic gigametre (Gm^3), about three-quarters of it in South East Asia. The carbon pool of

Figure 1. Tropical distribution of histosols from the Harmonized World Soil Database (HWSD). Only histosols have fully saturated colours (maroon), all other soil classes are in faded colours (default HWSD colour ramp)

tropical peatlands is estimated to be 88.6 Gt (Page *et al.* 2011), which is higher than estimates in most previous studies.

The conversion of natural tropical wetlands to agriculture and agroforestry causes rapid subsidence and oxidation of peat accumulated in wetlands, with subsequent release of carbon to the atmosphere. The conversion of wetlands is especially intense in South East Asia (Gibbs *et al.* 2010).

The world's largest peatlands (in extent) are all situated on alluvial fans in tropical and sub-tropical regions. The largest is the Pantanal in South America, straddling the borders of Brazil, Bolivia and Paraguay (fed by the Paraguay River). This is followed in size by the Sudd in Sudan (fed by the White Nile) and the Okavango in Botswana (fed by the Okavango River). The Niger Inland Delta in Mali (fed by the Niger River) is partly converted to agriculture, but was originally larger than the Okavango. The Niger Inland Delta is reported to have shrunk from 37 000 km^2 to 15 000 km^2 between 1950 and 1990 (Niasse *et al.* 2004). Landmann *et al.* (2010), in a recent study using moderate resolution optical satellite imagery, estimated the area of the Niger Inland Delta wetland at about 9000 km^2. McCarthy *et al.* (2003) showed that the flooded area of the Okavango Inland Delta (Botswana) has varied considerably in historical times, but put the present area of the Okavango wetland at about 9000 km^2. The considerable variations in area of these large wetlands, as well as the rapid conversion of wetlands to agriculture and agroforestry, call for new and rapid methods for mapping global wetlands.

1.1 Wetland mapping

Wetlands are almost universally shown on topographic maps. Topographic maps stemmed from military needs for information on terrain, and the location of wetlands was important. Hence, the coverage of wetlands on topographic maps is usually good. But topographic maps only cover parts of the tropics and only very restricted areas are openly accessible in digital form. Thematic maps, and generalised maps, on smaller scales than traditional topographic maps, very seldom include information on wetlands, even if they are easier to access. Many remote regions, including the world's largest tropical forests in the Amazon Basin (South America) and the Congo Basin (Africa), have never been properly ground surveyed. Recent studies using satellite images show that both the Amazon Basin (e.g. Lähteenoja *et al.* 2012) and the Congo Basin (Bwangoy *et al.* 2010) contain large areas of wetlands. These studies indicate that the total wetland area of the tropics might be larger than hitherto estimated.

Global mapping of the earth's land surface from earth observing satellite (EOS) images has mainly focused on land cover and topography. Global thematic maps which show wetlands are still mostly based on data compiled from national surveys and are usually at scales of 1:1 million (1:1M) or coarser. The most useful map of the global land surface might still be the Digital Chart of the World (DCW); the 1:1M operational navigation chart developed by the United States Defence Mapping Agency. The DCW does show wetland classes, but they are not reliable and cannot be used as a basis for estimating global tropical wetlands. Some of the global land cover maps developed from EOS images do show wetland classes. These global maps, however, focus primarily on vegetation classes, and, hence, most tropical wetland areas are categorised as forest, shrubland or grassland. Figure 2 shows the moderate resolution imaging spectroradiometer (MODIS) global land cover product (MCD12Q1) (Friedl *et al.* 2010). Version 051 of the MODIS land cover product uses a

Figure 2. The standard MODIS land cover product (MCD12Q1 version 051) for 2010. Permanent wetlands have a fully saturated (blue) colour; other land cover classes have the default hue used for the International Geosphere-Biosphere Programme classification scheme of MCD12Q1, but with faded saturation

decision tree classification algorithm that is iteratively improved by comparing results against a validated set of training data.

The European Space Agency (ESA) GLOBCOVER map at 300 m resolution (Figure 3) also attempts to show global tropical wetlands (Bontemps *et al.* 2010). GLOBCOVER is primarily based on time series data from the medium resolution imaging spectrometer (MERIS) sensor on board the ESA ENVISAT satellite. GLOBCOVER combines more traditional image analysis techniques and relies on extensive ground control points. The wetlands classes are partly derived from a combination of the MERIS classification scheme and ancillary data. A third global land cover map is the ESA Global Land Cover 2000 map. This latter map is a compilation of various efforts and has not been used in this study. The only globally reliable map of wetlands available is the recently published global mangrove map (Giri *et al.* 2011).

When comparing the global land cover maps for Africa, Kaptué Tchuenté *et al.* (2011) concluded that large scale features were well captured, but that the heterogeneous landscapes deserved more attention. They suggest that timing and phenology could improve the classification of heterogeneous landscapes.

Global land cover products have been directed towards identifying vegetation classes and, though they include wetland classes, the soil substrate has been largely ignored. Global soil maps, in contrast, lack detailed information from many parts of the globe (FAO *et al.* 2012), and are too generalised to be used for identifying global tropical wetlands (cf. Figure 1).

1.1.1 Optical EOS images

Wetlands are easy to identify from a ground survey, but are more difficult to discern in satellite images. This is especially the case if the vegetation cover is dominated by trees or if the wetland is a regularly flooded plain, which is either wet or dry, but is not persistently very wet throughout the year. Green *et al.* (1998) summarise the most common methods for mapping mangrove wetlands using EOS images. They divide techniques for wetland mapping using optical EOS images into six categories:

1. Visual interpretation
2. Vegetation index based classification
3. Unsupervised statistical classification
4. Supervised statistical classification
5. Statistical classification from band ratio indices or linearly transformed indices
6. Merged or combined classification.

Almost all attempts to map wetlands using optical EOS images take one of these six approaches. A merged or combined classification technique will generally produce the most accurate classification, but will also be the most time consuming and costly. The best results are reported in studies which have used manual approaches, or a combination of manual and automated (statistical) approaches. The recently published global map of mangroves (Giri *et al.* 2011) combined manual and unsupervised statistical methods to identify mangrove from approximately 1000 Landsat scenes. More than 30 Ph.D. students from the tropics and sub-tropics were involved in the classification. Most wetland mapping studies using optical EOS images are restricted to ecologically and climatically homogenous regions, where the use of the first five methods listed above is appropriate. The assumptions underlying methods 2 to 5 are that similar features (wetland categories) can be mapped using reference data and that there is statistical similarity in one or more bands. The bands can be spectral data, a vegetation index, or some other index derived from band rationing or band linear transformations and combinations, for example principal component analysis (PCA). The basic assumption of similarity is eroded when adopting methods 2 to 5 over extended regions. Differences in species composition, soil conditions, and local and

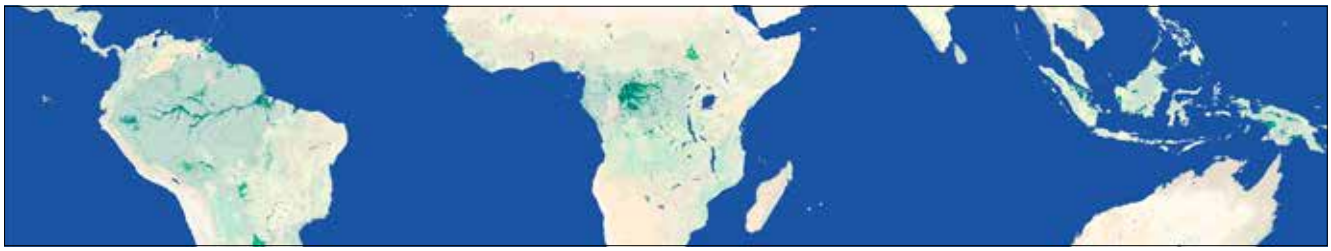

Figure 3. ESA GLOBCOVER 2009 version 2. All classes are shown by the default hue, with faded saturation for all classes except wetlands

annual climate cycles prevent a statistical approach based on similarity. One tractable alternative is to use time series data and adjust the classification based on the local phenology of climate, surface wetness and vegetation. Landmann *et al.* (2010) used time series MODIS data to identify West African wetlands from the phenological characteristics of vegetation. But their approach also used extensive ground data for calibrating the image classification.

1.1.2 Radar EOS images

All radar data have the advantage of being more or less unaffected by atmospheric conditions (including clouds). The shorter radar wavelengths (C-band) are scattered by leaves, woody biomass and water. Hence, radar is widely used for biomass mapping. The longer radar wavelengths (L-band) are less affected by leaves and penetrate herbaceous biomass. The L-band is commonly used for mapping woody biomass and surface wetness conditions. Hence L-band radar, in particular, has led to advances in wetland mapping (Costa *et al.* 2007; Hoekman 2007). The interpretation of surface (water) conditions from radar data is, however, not straightforward. The backscatter received by the satellite sensors – usually expressed as a normalised measure, sigma nought (σ_t) – is a composite of scattering from at least four components (Wang *et al.* 1995):

$$\sigma_t = \sigma_s + \sigma_c + \sigma_m + \sigma_d$$

where
σ_s is the direct canopy backscatter,
σ_c is the canopy volume backscatter,
σ_m is the canopy and ground interactive backscatter and
σ_d is the double bounce backscatter.

As radar images are usually taken at a steep angle of incidence (and not perpendicularly), open water surfaces deflect the radar signal away from the sensor, and the return signal from a smooth (calm) water surface will be extremely low. A dense forest will have a higher backscatter than any other vegetation type (composed of all four scatter components). If the ground in the forest is flooded the backscatter will increase even more, as a consequence of the double bounce (σ_d) component.

However, when an herbaceous plain (e.g. a floodplain dominated by grassland) is flooded, the water surface will deflect the scatter away from the sensor, and the backscatter recorded by the satellite sensor will be lower than under non-flooded conditions. The type, height and volume of the vegetation will hence determine how the backscatter changes with variations in surface wetness. Thus, when using L-band radar the relative variations in backscatter over time can be used as indicators of changes in surface wetness (Wang *et al.* 1955). But interpreting the absolute wetness still demands calibration against ground data. By measuring not only the backscatter, but the polarisation of the backscatter, a multi-band approach can be used to map wetlands from either a single radar scene, or from a time series of radar scenes.

1.1.3 Topography

An alternative digital data source for mapping wetlands is to use a digital elevation model (DEM). From a DEM the drainage area (the upstream area feeding into a given position) for each cell or picture element (pixel) can be used to represent the amount of water that flows into the cell. This, combined with the local slope or curvature of the cell, enables a topographic index – a proxy for the local wetness – to be defined (Beven *et al.* 1979). Variants of the topographic index have been used to map wetlands in different environments. In their study of wetlands in the central Congo Basin, Bwangoy *et al.* (2010) concluded that the local drainage area, derived from topographic data, was the most important information for mapping the distribution of wetlands.

1.2 Approach

Tropical wetlands change in size because of natural climatic fluctuations and as a consequence of human management. To map global tropical wetlands, the only feasible approach is to use EOS image data. As discussed above, traditional statistical image classification techniques cannot be used to map wetlands over extended regions because of large seasonal variations in time and space in flooding and vegetation phenology. Existing global land cover maps are based on advanced (iterative) statistical approaches, relying on large sets of verified ground control data. For wetlands, the lack of globally relevant and verified ground control data prevents the use of statistical approaches for generating a global wetland map. As wetlands are 'lands transitional between terrestrial and aquatic systems', they are almost, by definition, heterogeneous and global

scale land cover maps are more error prone in heterogeneous areas. Further, wetlands and peatlands are defined by soil, not vegetation, conditions. Taking this into consideration, this study developed an alternative approach for mapping global tropical wetlands.

The first stage was to develop a set of physically intelligible indices and maps that have a logical relationship to the distribution of wetlands. The indices include: A global topographic wetness index; A global surface wetness index derived from optical EOS images; A global geomorphological map; A third surface wetness index, derived from radar data, was also developed, but was not adopted because of geometrical position errors in the radar data set. The phenology (annual cycle) of surface wetness was extracted from the optical surface wetness index. By combining the information on surface wetness phenology, topographic wetness and geomorphology, areas that are more or less likely to harbour wetlands can be identified.

The second stage was traditional image classification using a chrono-sequence of images for extracting phenologically relevant reference signals for use in image classification in defined spatial and temporal domains. Because of the lack of verified reference sites, the second stage could only be tested for selected regions and a limited number of wetland classes. However, the lack of verified data, even for this limited number of regions, prevents accurate estimates.

2. Objectives

The present best estimates of global topical wetlands are derived from compilations of disparate source information from studies using a variety of different techniques. The primary objective of this study was to develop a credible map of global tropical wetlands.

3. Data sets

The core data compiled for this study consists of products from the MODIS sensor. A range of pre-defined products derived from the MODIS sensors are available on the internet with free file transfer protocol access. All MODIS products used in this study are delivered in a pre-defined tiling system (Figure 4). Each tile represents approximately a 10° by 10° (at the equator) segment of the earth's surface. For this project 83 tiles, representing the tropical land surface of the earth, were selected. The study area includes the region between 25° north and 25° south. This is equivalent to vertical tiles 07 through 11 of the MODIS data products.

The native sinusoidal grid of the MODIS products provides wall-to-wall coverage of the entire earth's surface, and is an equal area projection. This is extremely advantageous when processing tiled images, and especially when modelling water balances. Hence, all processing was done using the MODIS sinusoidal grid. All non-MODIS data sets were cut and re-projected onto the MODIS pre-defined tiling system.

3.1 MODIS products

3.1.1 MCD43A4 – NADIR BRDF-adjusted reflectance data 16-day L3 global 500 m

The MODIS product MCD43A4 consists of seven bands ranging from the visible to infrared wavelengths. The reflectance in each wavelength is corrected using a bidirectional reflectance distribution function (BRDF), and the values represent nadir reflectance. The complete annual time series for 2011, plus the last four dates of 2010 and the first four dates of 2012, were used in this study. The MODIS BRDF reflectance data is the most important data set in this study. It was used to identify spectral end-members, for defining and creating a novel set of indices related to wetlands, for pixel un-mixing of soil and vegetation, and for classification of wetlands. The version used was 005.

3.1.2 MOD13Q1 – vegetation indices 16-day L3 global 250 m

The MODIS vegetation product MOD13Q1 data set consists of four bands (red, near-infrared, blue and short wave infrared), and two vegetation indices – the classical normalised difference vegetation index (NDVI) and the enhanced vegetation index (EVI) – as well as metadata layers for quality and acquisition details. The complete annual time series for 2011, plus the last four dates of 2010 and the first four dates of 2012 were used in this study. Apart from using MOD13Q1 to extract vegetation phenology, the quality layer was used to extract lakes, shorelines and areas of intermittent inundation. The version used was 005.

3.1.3 MCD12Q1 – land cover type yearly L3 global 500 m

The annual MODIS land cover product MCD12Q1 is derived from an annual series of MODIS data. At the time of acquisition, the latest year for which land cover was available was 2009. The land cover product was used as a reference data set for vegetation types and as a background when visually inspecting processing steps and results. The version used was 051.

3.1.4 MOD44B – vegetation continuous fields yearly L3 global 250 m

The MODIS vegetation field product MOD44B, standard tree cover (%), is an annual product based on combinations of vegetation and reflectance data.

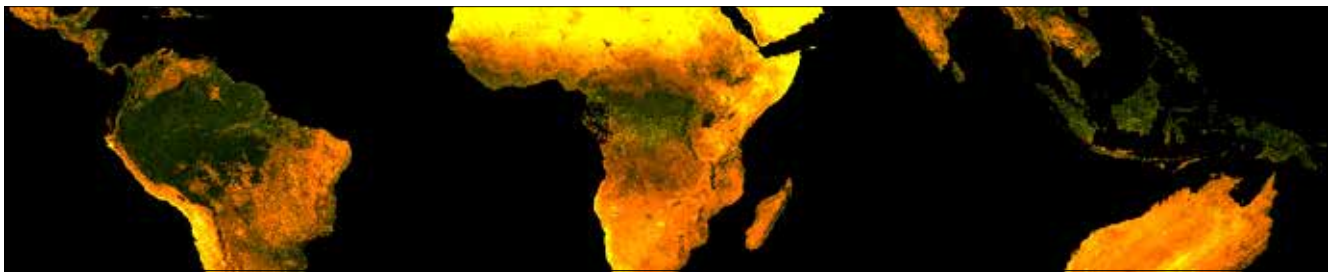

Figure 4. Tropical regions included in this study (colour composite of MODIS reflectance data for the peak of the dry seasons)

At the time of acquisition, the latest year for which land cover was available was 2010. The tree cover data was used for classifying wetlands types, and for validating results of intermediate processing steps in the definition of wetland related indices. The version used was 005.

3.2 Phased array type L-band synthetic aperture radar (PALSAR) data sets

The Japanese Aerospace Exploration Agency (JAXA) has, through its Kyoto and carbon (K&C) initiative, released global PALSAR data (horizontal transmitting, horizontal receiving and horizontal transmitting, vertical receiving bands) in 500 m resolution. For tropical forested areas (outside South America) the K&C initiative has also published PALSAR data in 50 m resolution. Both data sets were retrieved and organised into the MODIS tiling system. Algorithms for the mapping of flooding and inundation from time series data have been implemented, as well as land cover classification routines using multi-band backscatter data. The geometric precision of the PALSAR 500 m product (that covers the whole tropics) was, however, found to suffer from substantial errors. Hence, the present study does not present any results from the PALSAR sensor.

3.3 Ancillary data set

3.3.1 Topography

For this study Version 4 of the Shuttle Radar Topography Mission (SRTM) DEM, prepared by the International Center for Tropical Agriculture (CIAT) and available for download in approximately 250 m resolution, was used. This SRTM was cleaned for pits and all data points falling on land are filled. The absolute error of the SRTM data set is estimated to be 11.25 m, with a relative height error for adjacent pixels estimated to be 1.6 to 3.3 m (Brown *et al.* 2005). The SRTM data was re-sampled to the MODIS sinusoidal grid with a 250 m spatial resolution using a bilinear interpolation. The topographic data was used to extract a set of geomorphological indices, and combined with climate data to derive a topographic wetness index which was used to map the distribution of global topographic wetland.

3.3.2 Precipitation and temperature

Precipitation and temperature were taken from the WorldClim database, version 1.4, release 3 (Hijmans *et al.* 2005). The WorldClim database contains monthly interpolated grids of about 1 km^2 (30' of arc) spatial resolution representing precipitation, minimum and maximum temperatures. The spatial data represents the period 1960 to 1990, extended from 1950 to 2000 for regions with poor data coverage 1960 to 1990. The station data used is a compilation of globally available climate station data. Interpolation of the original WorldClim data set was done using thin plate smoothing splines. For this project the precipitation data was re-sampled to the MODIS sinusoidal grid with a 250 m spatial resolution using a bilinear interpolation. The annual time series of precipitation was used to extract local phenological patterns, including defining dates (Julian day of the year) for wet and dry seasons.

3.3.3 Evapotranspiration

Evapotranspiration values were taken from the FAO-adopted monthly reference evapotranspiration values produced by the Climate Research Unit, University of East Anglia (New *et al.* 2002). The evapotranspiration data was re-sampled to the MODIS sinusoidal grid with a 250 m spatial resolution using a bilinear interpolation. The evapotranspiration data was combined with the precipitation data to derive a water balance model. The water balance model was then used in conjunction with the topographic data to define a global topographic wetness index (GTWI).

3.3.4 Harmonized world soil database (HWSD)

The HWSD is a regularly updated product. The data set used in this study was version 1.2.1, updated on 7 March 2012 (FAO *et al.*, 2012). The dominating soil group and the top soil organic carbon content (%) were extracted from the HWSD database and re-sampled using the nearest neighbour to fit the MODIS tiles. The result was visually compared with the results obtained from various processing steps. The coarseness of the HWSD data meant it could not be used to statistically calibrate or validate algorithms at the spatial resolutions used in this study.

3.3.5 GLOBCOVER

GLOBCOVER is the highest resolution (300 m) global land cover product presently available. The GLOBCOVER initiative is a joint effort led by the ESA, and mainly uses images acquired from the MERIS sensor on board the ENVISAT satellite mission. The version used was GLOBCOVER 2009 (Bontemps *et al.* 2010).

4. Methods I – climate and topography

4.1 Climate phenology

4.1.1 Background

The formation and distribution of wetlands is very dependent on annual precipitation and inundation/flood cycles. Most tropical regions are characterised by high temperatures and a pronounced annual rainfall cycle. Tropical rainfall is largely governed by the Inter-tropical Convergence Zone (ITCZ) – the low pressure zone girdling the earth at the solar zenith latitude and oscillating between the tropics. The low pressure zone attracts surface winds and, if the winds are moisture laden, precipitation is generated. Hence, in the tropics there is a single pronounced annual rainy season (in the hemispherical summer), whereas the equatorial region has two annual rainy seasons. The seasonality of the rainy season(s) is mirrored with six month lags at similar latitudes north and south of the equator. Thus the annual precipitation phenology is very different in the northern and southern hemispheres, and close to and away from the equator. The flooding and inundation cycles of individual tropical wetlands depends on both their location and on the location of their drainage basins.

When analysing wetlands from satellite images, the large variations in precipitation and surface inundation/flooding phenology must be accounted for. For example, wetlands north and south of the equator cannot be mapped based on the same date and reference spectra and the same is true for wetlands close to and further away from the equator. Additionally, the ITCZ is not positioned at a precise latitude, but is attracted towards large (warm) land masses; it wiggles in its position girdling the globe. Hence, reference data on wetlands from one continent cannot be easily used to map wetlands on other continents.

In essence, the large variations in annual precipitation and inundation phenology require a knowledge of local phenology prior to attempting a global classification of wetland distribution.

4.1.2 Annual precipitation phenology

Annual precipitation phenology was calculated from the WorldClim data set (Hijmans *et al.* 2005). The following ten indices were calculated for each pixel at a 250 m spatial resolution:

1. Monthly minimum rainfall (min)
2. Monthly maximum rainfall (max)
3. Monthly mean rainfall (mean)
4. Date of the maximum rainfall or peak of the wet season (pws)
5. Date of the minimum rainfall or peak of the dry season (pds)
6. Threshold between dry and wet season(s) (dwt)
7. Number of wet (dry) seasons (nrpeaks)
8. Date of the start of the wet season following the longest dry period (sws)
9. Date of the start of the dry season following the longest wet period (sds)
10. Length of the wet season(s) (lws).

The threshold between wet and dry seasons (dwt) was set as:

$$dwt = 0.5 * (mean - min) + min$$

The setting of a relative threshold assures that all regions with a precipitation cycle (i.e. all areas except deserts) will be accounted for. The volume of precipitation defining the threshold between wet and dry seasons, will, however, vary greatly.

Computationally the volume indices (mean, minimum and maximum) were calculated directly from monthly data. For the temporal indices (pws, pds, dwt, nrpeaks, sws, sds and lws) the WorldClim precipitation data was interpolated to represent 23 dates instead of the original 12. Under the assumption that the WorldClim data set represents the precipitation of the mid-day of each month, the interpolation was done so that the 23 new dates represent the mid-days of the 16-day periods used in the two MODIS products (MOD13Q1 and MCD43A4). This was done to facilitate extraction of seasonal spectral signatures (and derived indices) representing the various stages in the annual precipitation cycle. Figures 5 through 13 show the global precipitation phenology derived from the WorldClim data set.

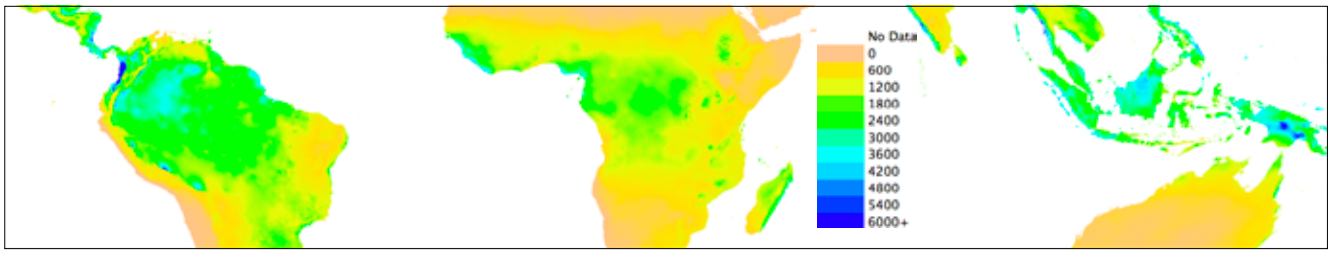

Figure 5. Annual average precipitation (mm) re-scaled to the monthly average to correspond to the maps below

Source: WorldClim

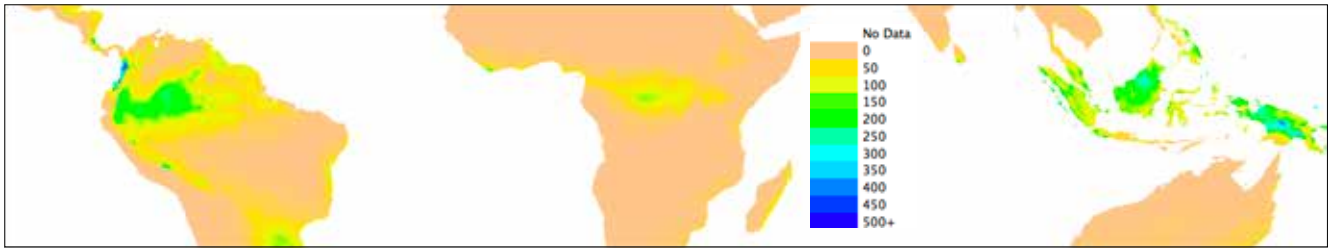

Figure 6. Monthly minimum precipitation (mm)

Source: WorldClim

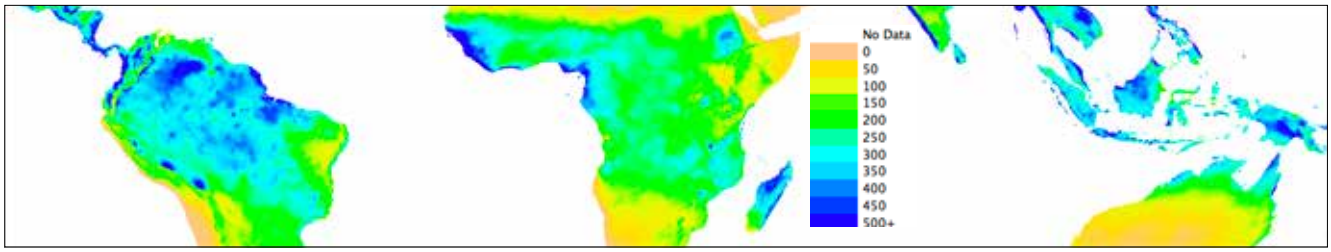

Figure 7. Monthly maximum precipitation (mm)

Source: WorldClim

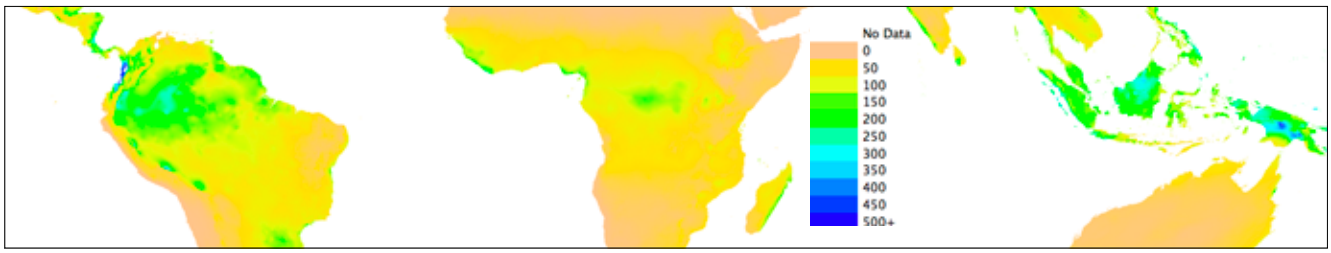

Figure 8. Precipitation threshold used for separating dry and wet seasons (mm)

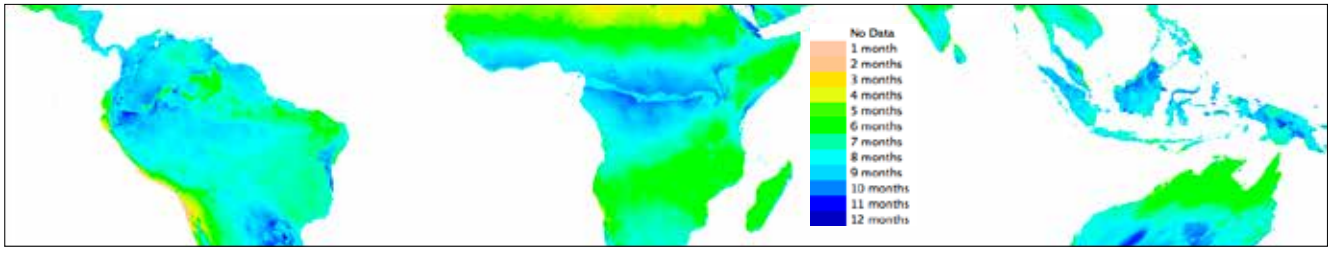

Figure 9. Length of wet season (months)

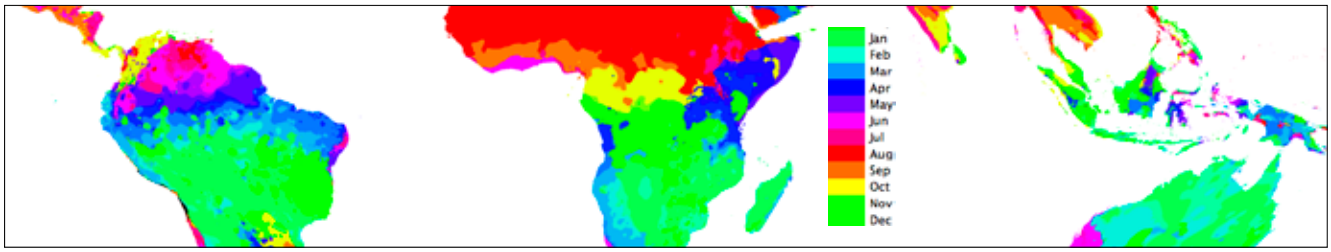

Figure 10. Date of the peak of the wet season

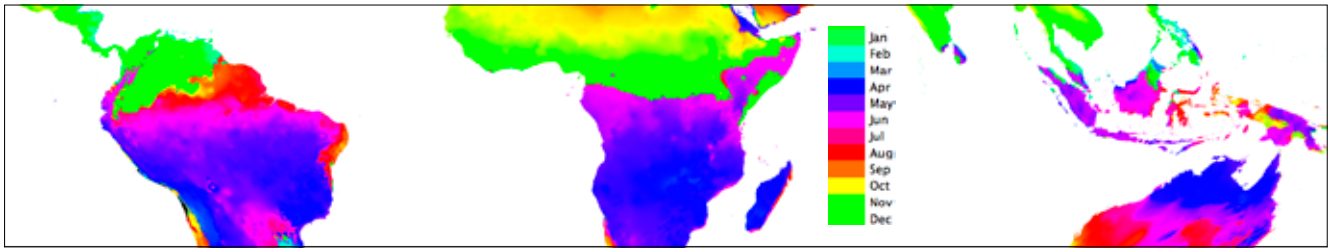

Figure 11. Date of the start of the dry season

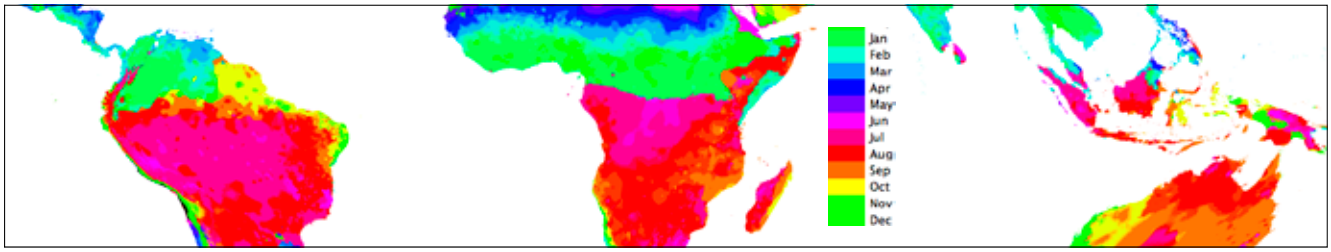

Figure 12. Date of the peak of the dry season

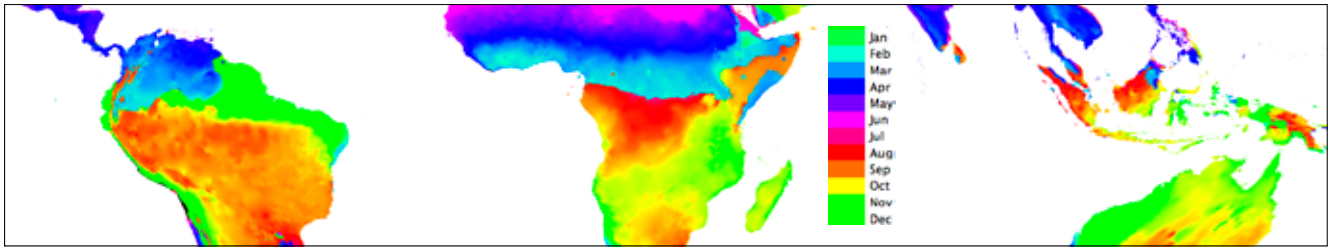

Figure 13. Date of the start of the wet season

4.2 Topographic wetness

4.2.1 Background

Topography influences the gravitational flow of water over and through the landscape. Landforms control the hydraulic head, water flow and water distribution. Conceptually, soil water transmissivity determines the volume of water driven by the topographically induced hydraulic head. In temperate climates, soil transmissivity, in general, increases towards the soil surface. During rainfall, the groundwater level rises and the water saturated lower slope area expands. This leads to storm flow (Hewlett and Hibbert 1967). This transmissivity feedback mechanism and the spatial variation in the saturation (or source) area generating runoff, has led to various approaches that use topography as a proxy for estimating the spatial distribution of hydraulic head and wetness. The most widely adopted algorithm for translating topographic information into landscape hydrological responses is the topographic index (Beven and Kirkby 1979; Quinn *et al.* 1995). The topographic index was originally developed for a dynamic hydrological model, TOPMODEL (Quinn and Beven 1993). In its original form, the topographic index was based on at least the following assumptions: Rainfall is equal over the drainage area The slope equals the hydraulic gradient of the groundwater table. Water transmissivity increases exponentially towards the

soil surface and is equal over the drainage area. Soil wetness can be represented as a series of steady state conditions. There is no unsaturated lateral flow.

The topographic index is defined as:

$$I = \ln\left(\left(A/b\right)/\tan\beta\right)$$

where A is the upstream catchment area, b the contour length, and β is the local slope steepness in degrees.

By setting $\alpha = A/b$, the TOPMODEL topographic index is usually given as:

$$I = \ln\left(\alpha/\tan\beta\right)$$

In principle the index will take on a higher value as the upstream catchment grows and the local slope angle flattens.

In tropical climates the transmissivity feedback hypothesis of higher water conductivity towards the soil surface is less well established. Tropical soils are often deeper, older and more weathered than temperate soils, and were not formed by glacial forces, but rather by *in situ* processes. And, as discussed above, precipitation patterns in the tropics varies substantially. Thus, adopting the topographic index for dynamic rainfall to runoff modelling in tropical landscapes is not straightforward. The gravitational influence on the water flow is, however, based on primary physical principles, and the landscape average or long term wetness condition is strongly influenced by topography also in tropical landscapes. For example, in a recent study in the central Congo Basin, Bwangoy *et al.* (2010) found that the upstream area was the most decisive factor for mapping the distribution of wetlands.

Many attempts have been made to both improve and generalise the topographic index. Merot *et al.* 2003 introduced effective rainfall (total rainfall less evapotranspiration) as a factor, and derived the climato-topographic index:

$$I = \log\left(Vr/\tan\beta\right)$$

where Vr is the volume of water supplied by the upstream catchment to the local pixel. This is derived by multiplying the effective rainfall by the upstream area. Merot *et al.* (2003) applied the climato-topographic index across climate gradients in Europe and concluded that it could predict wetland distributions without local calibration.

A second development of the TOPMODEL topographic index has been to replace the local slope angle, β, with an angle or factor that relate to the down slope condition, or profile curvature – with convex slopes being drier and concave slopes wetter. Crave and Gascuel-Odoux (1997) showed that the downstream geomorphology had a larger influence on wetness than the local slope, and suggested that the local slope should be exchanged for the slope towards the nearest drainage point. Following Hjerdt (2004), the down slope influence in several studies has been defined as the horizontal distance along the slope gradient needed for the elevation to drop a user defined value (Rodhe and Seibert 1999). In the latter modified TOPMODEL topographic index, the slope factor can be expressed either as a distance L_d [m], or as a gradient:

$$\tan\alpha_d = \frac{d}{L_d}$$

where L_d is the horizontal distance to the nearest point with an absolute elevation d m below the local cell under consideration.

Hjerdt (2004) showed that this modified topographic index could overcome some of the shortcomings reported by other studies when using the original TOPMODEL topographic index for mapping soil moisture and groundwater levels in complex topographic terrains. The $\tan\alpha_d$ factor is also reported to be less scale dependent than $\tan\beta$, but demands a calibrated setting of d.

Rodhe and Seibert (1999) tested both the original and the modified TOPMODEL topographic indices to map distributions of mires in small Swedish catchments, and showed that wetlands not connected with the stream network could be identified, but with moderate success. In adopting the original TOPMODEL topographic index for mapping wetlands in the Seine Basin, France, Curie *et al.* (2007) concluded that it was applicable also in basins with large aquifers (groundwater reservoirs) dampening the rainfall to runoff process.

4.2.2 Data pre-processing

Identifying a global tropical topographic wetness index requires pre-processing both topographic and

climatic input data. The following must be calculated from the DEM:

- Stream and river network (as conduits of surface water flow)
- Drainage network (water flow over hill slopes)
- Slope angle at different resolutions
- Profile curvature at different resolutions
- Flow accumulation.

From the climatic data, the fraction of the runoff generated by annual rainfall must be calculated as the difference between the gross rainfall and evapotranspiration. The WorldClim precipitation and FAO-adopted evapotranspiration data sets only cover continental areas; some coastal strips fall outside the data coverage. These strips were filled by expanding the original data sets using the nearest pixel value to grow the climate grids to fill all land areas.

The term 'effective rainfall' is widely used in hydrological studies and defined as the fraction of rainfall that is not lost by evapotranspiration but which forms downstream flow and runoff. The term effective rainfall is a troublesome misnomer which has led to many ill-formulated concepts in hydrological science. It is, however, so well established that it is difficult to get rid of. From an ecological (or thermodynamic) perspective it is the runoff that is the loss and the evaporated fraction that is effective (Gumbricht 1996). One can even speculate that this misnomer has hindered novel developments in the hydrological sciences, such as the formulation of better topographic wetness indices. In this study, the fraction of gross rainfall that is not lost by evapotranspiration will be called runoff rainfall (*Rrun*). The fraction that is (in due time) lost by evapotranspiration will be called evaporative rainfall (*Ret*). For regional estimations of rainfall to runoff generation , *Rrun* is useful for calculating runoff volumes, but for local wetness and water cycle conditions it is hypothesised that the *Ret* fraction might be of equal or even greater importance.

4.2.3 Extraction of streams, rivers and drainage networks

Streams, rivers and lakes are conduits of open water flow, and do not constitute wetlands. Stream and river networks were extracted by applying the single flow direction (SFD) algorithm to the SRTM DEM. The SFD finds the elevation difference between a central cell and each of its eight nearest neighbours and assigns the pathway towards the steepest descent. The calculation was done using the terraflow algorithm (Arge *et al.* 2003). The global tropics were divided into eight overlapping areas (Central America, South America, West Africa, North Africa, South Africa, Central Asia, South East Asia and Australia), each defined so that all tropical basins were completely analysed within one of the areas. Lakes were extracted by combining the quality layer from the MODIS vegetation product (MOD13Q1 version 5), with the SRTM. Flat areas identified from the SRTM and indicated as inland water in the MOD13Q1 quality layer were categorised as lakes.

The multiple flow direction (MFD) algorithm distributes the flow accumulation from the central cell to all of the eight closest neighbours which have a lower elevation; the outflows are assigned proportional to the slope angle to these lower lying neighbours. The MFD is better suited for realistic calculations of upstream areas along hill slopes and is superior for topographic wetland mapping (Quinn *et al.* 1991; Wolock and McCabe Jr. 1995). Hence the MFD was used for calculating the contributing area (A_u) to each cell outside the stream, river and lake network. Also the MFD flow accumulation was calculated using the terraflow algorithm of Arge *et al.* (2003) and eight overlapping parts. To convert the contributing area (A_u) derived from MFD to the topographic parameter α, the contour length (b) was set to the length of the side of a cell.

$$\alpha = A_u / b$$

In the calculations, the contributing area (A_u) is measured in m^2 and the contour length (b), in metres. Hence the unit of α, is metre [m].

4.2.4 Slope and curvature

The slope and curvature of a particular position depends on the scale of the DEM from which it was calculated. In general, both slope and curvature flatten out as the spatial resolution of the cell increases. Analysing slope and curvature at hierarchical scales also allows the derivation of landforms from a DEM (see below). In this study the original DEM has a 250 m spatial resolution. To map landforms and slope positions, the DEM was re-sampled to four coarser resolutions; 750 m, 1500 m, 3000 m and 6000 m. For each hierarchical scale, the morphology was characterised by a profile curvature and slope, as defined by Wood (1996).

4.2.5 Runoff generating rainfall

Runoff rainfall (*Rrun*) was derived by summing the positive differences between total rainfall (*P*) and reference evapotranspiration (*ET*) for each month (*m*):

$$Rrun_{annual} = \sum P_m - ET_m, \; when \; P_m > ET_m$$

Monthly precipitation was taken from the WorldClim global data set (Hijmans *et al.* 2005). This represented the average precipitation for approximately 1950 to 2000. Evapotranspiration was taken from the FAO-adopted monthly reference evapotranspiration, produced by New *et al.* (2002). Figure 14 shows the annual runoff rainfall.

4.2.6 Adopting a topographic wetness index for tropical wetlands

Initial attempts to identify tropical wetlands from the original TOPMODEL topographic index failed. Multiplying the cell upstream drainage area (A_u) by the runoff forming fraction of the rainfall ($Rrun_{annual}$) improved mapping, but still failed to account for wetlands as diverse as the tropical peat dome forests on the one side, and flooded-out rivers forming alluvial fans with peat on the other. Runoff rainfall in the former can be several metres per year, whereas the latter can be situated where there is not a single month when precipitation exceeds evapotranspiration.

Using an empirical trial and error approach, first the direct local (cell) precipitation was considered as contributing towards sustaining the wetlands (or rather the near surface groundwater table). Mathematically, the rainfall was converted to metres as the water volume (precipitation x cell area) and dispersion area (cell area) cancel out. Obviously this climato-topographic index ($\ln(Vr/\tan\beta)$) has the unit ln(m^2), and the local precipitation, the unit ln(m), and thus they cannot be directly compared. The simplest solution is to take the square root of the contributing area (A_u), thus converting also the climato-topograpic index to the unit ln(m). This conversion of the climato-topographic index gives a very much better prediction of wetland distribution throughout the global tropical region.

Minor local wetlands are less well captured by combining the local (cell) water contribution and the upstream water contribution. Hence a third water contributing component was added – the local water flow from adjacent cells. The contribution from adjacent cells was calculated using the local geomorphology. To keep the mass balance of water, the flow of water between adjacent cells was calculated from the evaporative fraction (*Pet*) of precipitation. The contribution from adjacent cells can be viewed conceptually as the unsaturated flow prior to evapotranspiration. Inclusion of this third water contribution factor generates a global wetness index which visually corresponds well with the global distribution of tropical wetlands, ranging from peat dome forests to alluvial flood plains. Over extremely flat terrain (i.e. large alluvial fans), the accuracy of the SRTM cannot resolve flow paths and, for such environments, the topographic index fails.

4.2.7 Inductive theoretical considerations

Precipitation across the global tropics varies in the extreme, from virtually no precipitation (the Sahara) to precipitation in excess of 5000 mm per year. Under these circumstances, and considering the reported efficiency in wetlands mapping adopting the climato-topographic index, the inclusion of rainfall (flow volume) for mapping global tropical wetlands is deemed to be essential.

The climato-topographic index was developed for temperate climates, where rainfall is commonly much greater than evapotranspiration. In the

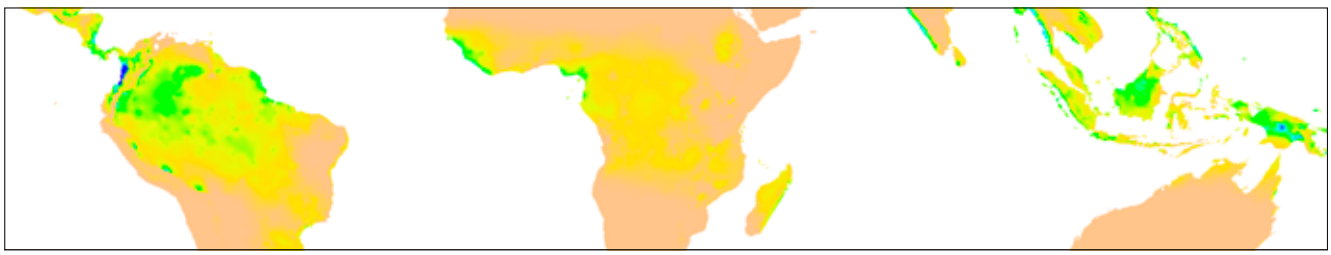

Figure 14. Annual runoff generating rainfall (precipitation – evapotranspiration) (mm) re-scaled to the monthly average to correspond to the maps above

tropics, evapotranspiration often exceeds rainfall, but despite this, wetlands do form in areas with no or little efficient rainfall. In general these wetlands are fens, mainly supported by upstream water inflow from areas with higher rainfall, but the extent and sustenance of fens also depend on local rainfall (even if that water in due time is lost by evapotranspiration). Local rainfall in regions with no efficient rainfall supports wetlands; rain falls directly on the wetlands and water accumulates in depressions prior to evapotranspiration. Thus the contributions of the gross local and neighbouring rainfall cannot be neglected when mapping the global distribution of tropical wetlands from climatic and topographic data.

In traditional hydrological studies, the runoff rainfall (*Rrun*) is the only water component considered when mapping, for example, groundwater levels and wetlands. As noted above, the fraction lost by evapotranspiration is the fraction used by vegetation, for example, for driving photosynthesis, root nutrient uptake and surface cooling. If we, for instance, assume that gross precipitation and potential evapotranspiration are in perfect balance, the soil will be completely water saturated if permitted by the topographic setting – but the climato-topographic index will be 0. This suggests also that precipitation that is later lost by evapotranspiration contributes towards sustaining wetlands. Moreover, wetlands are not seldom situated in depressions that collect surface and unsaturated flows (or saturated overland flows) during storm events – even if the runoff rainfall (*Rrun*) is negligible on average. Rather, for local hydrological studies, the gross rainfall is distributed between three (and not two) fractions – the fraction directly lost by evapotranspiration at the local scale (the cell size chosen in the study), the runoff fraction and a third fraction that flows to adjacent cells prior to being lost by evapotranspiration. The latter fraction will be small on flat terrains (and have the character of an exchange rather than a uni-directional flow), but will increase as the terrain steepens. Also it will be scale dependent; smaller cells will tend to export a higher fraction compared to larger cells.

Replacing local slope steepness ($\tan \beta$) with slope curvature (e.g. $\tan \alpha_d$) is a logical approach for regions where the soil transmissivity is more homogeneous with depth and the hydraulic head does not directly link to the local slope. The different approaches taken to modify $\tan \beta$ to represent slope curvature have focused on downstream conditions. Using the profile curvature along the steepest gradient itself is a more direct approach. It is also computationally faster when analysing massive DEMs.

If conditions are right, wetlands in the montane tropics can exist on slopes of up to 10° (Trettin 2012). In such conditions the slope steepness does not limit wetland development primarily through wetness, but by flow-induced shear stress exerted on both the plant community and the accumulated organic matter. The local slope angle is hence important, but for reasons other than determining wetness.

4.2.8 Defining a global topographic wetness index for the tropics

Considering the difference in soil properties and climate between temperate and tropical regions, a four pronged approach to estimating surface wetness in tropical regions was developed. The first part is the upstream water contribution, which is similar to the climato-topographic index proposed by Merot *et al.* (2003), but includes a distance decay function and redefines the flow volume to a flow vector – rainfall runoff x (square root of upstream area). The second part is the water contribution from neighbouring areas, where a part of the vertical water cycle (*Ret)* is assumed to reach adjacent cells prior to evapotranspiration, dependent on local geomorphology. Also this flow is considered a vector – hypothesised to represent the unsaturated flow. Both flow vectors are divided by the cell contour length (b) set to be equal to the side of the cell. The third part is the direct local rainfall falling on a cell – regarded as a field. The three water contributions all have units in metres. The fourth part is the influence of the local slope and slope curvature, assumed to consist of two components – one component relating to slope curvature (wetness) and one component relating to absolute slope (shear stress).

The global topographic Wetness index (GTWI) is hence defined as:

$$GTWI = \ln\left[\frac{\left(\frac{Rrun * \sqrt{A_u}}{b} + \frac{Retadj * \sqrt{A_n}}{b} + Ret * 0.5\right)}{(\tan B * Curvfac)}\right]$$

where A_u is the upstream contributing area, A_n is the neighbouring contributing area, b is the contour length, *Retadj* is the fraction of (total precipitation

– efficient precipitation) falling on adjacent (neighbouring) cells that reach the local cell, *Ret* is the fraction of the local rainfall that is later lost by evapotranspiration, and *Curvfac* is a curvature factor (*Curvfac* = 1 when the curvature in planar, *Curvfac* <1 when the curvature is concave and *Curvfac* >1 when the curvature is convex)

The curvature factor was calculated as the curvature along the steepest descent as defined by (Wood 1996). The factor *Retadj* depends on the slope profile curvature at the local cell and its neighbourhood.

The GTWI is hydrologically balanced. The contributing upstream area (A_u) is calculated from the runoff rainfall (*Rrun*), excluding the local cell itself. The contribution from neighbouring cells is calculated from the fraction of the rainfall that is later lost by evapotranspiration (*Retadj*), and maximised to approximately 7 to 10% of this volume (dependent on geomorphology). From a single, high peak (at least 3 km wide, such as Mount Kilimanjaro) surrounded by valleys, the outflow fraction of the evaporative rainfall is 10% from the peak (and less from the slopes). The distribution of this outflow depends on the local geomorphology. Fifty per cent of the evaporative fraction (*Ret*) is added as a direct contribution to the local cell wetness. The contributing local neighbourhood is allowed to expand up to a maximum radius of 1.5 km (5 pixels). The amount of the local rainfall derived from neighbouring cells depends both on distance and curvature, with the closer and more concave curvature (of the receiving cell) contributing a higher fraction. The computational power needed to calculate the true local contributing area for each pixel is prohibitive. The approach used here is a simplification and involves using the slope curvature at four different scales: 250 m (original pixel resolution), 750 m, 1500 m and 3000 m. The wetness index does not generate any surplus water, but it allows some of the precipitation that is later lost by evapotranspiration to contribute towards local wetness.

4.3 Geomorphology

Wetlands only occur in specific geomorphological settings and some wetlands (notably peat domes) can change the local and regional geomorphology. Wetlands are both characterised by the geomorphology and characterise the geomorphology. The geomorphological setting can hence reveal additional information about the likelihood of wetlands occurring, the type of wetland and the depth and accumulation of organic matter taking place in a wetland.

Landforms are the result of the interaction between surface geomorphic processes (erosion, transport and deposition) and the underlying lithology. Over long periods, the geological cycle and plate tectonics determine large scale landforms. In between the processes of plate tectonics and micro-scale geomorphic processes, a range of hierarchical processes shape geomorphology (Short and Blair 1986). The largest tropical wetlands, for example, are all in tectonically active regions. Depressions formed as a result of the East Africa Rift Valley and the African Superswell are the foundations of the Sudd and the Okavango. The tectonic uplift of the Andes generated the geomorphology that subsequently delivered the material that forms the basement of the Pantanal.

The form of the land surface indicates the processes that formed it. Hence, a landform map can be used to interpret geomorphic processes, including soil and wetland formation. Landform maps can support the interpretation of other land surface characteristics, including hydrological properties and vegetation structure. The Soil Science Society of America (www.soils.org) defines a landform as "any physical, recognizable form or feature on the earth's surface having a characteristic shape, and produced by natural causes." This definition is broad enough for some authors to consider vegetation maps as a kind of landform map. Other definitions of landforms stress the more permanent nature of landforms, hence excluding vegetation cover as a landform class by itself. This latter definition will be adhered to in this study.

Most landform maps are either thematically bound to a particular biome, geographically restricted, or both. Thus many landform maps show a mixture of generic landform classes (e.g. lakes) and geographically bound (unique) landforms. Clements *et al.* (1957), for example, described 10 major landforms in the deserts of the world – alluvial fan, sand seas, playas, river plains, dry watercourses, mountains, recent volcanic depositions, low angle bedrock surfaces, desert flats and badlands. Ballantine *et al.* (2005) defined nine major landforms in the Sahara based on the map produced by Raisz (1952), and the definitions suggested by Clements *et al.* (1957) –

alluvial fan, dune fields, dry lakebeds, open water bodies, basaltic volcanoes and flows, sedimentary mountain ranges, regs, stripped bedrock surface and sand-sheets. Ballantine *et al.* (2005) used MODIS reflectance data and pixel un-mixing techniques to create a landform map of the Sahara using these major landforms.

Weiss (2001) developed a more generic landform classification scheme that can be extracted from DEMs. He based his classification on a multi-scale classification of the topographic position index (TPI):

$$TPI = Z_{grid} - focalmean(Z_{grid}, circle, r)$$

where Z_{grid} is the cell of the DEM, the *focalmean* is the mean DEM value within a circle of radius *r* centred on the cell.

By using TPIs derived from two (or more) hierarchical scales, a fairly simple set of rules can be used for classifying any landscape into 10 more basic classes (Weiss 2001):

1. Canyons, deeply incised streams
2. Mid-slope drainages, shallow valleys
3. Upland drainages, headwaters
4. U-shaped valleys
5. Plains
6. Open slopes
7. Upper slopes, mesas
8. Local ridges/hills in valleys
9. Mid-slope ridges, small hills in plains
10. Mountain tops, high ridges

Wood (1996) developed a set of primitive (cell) morphometric parameters that can be extracted from any DEM:

1. Elevation
2. Slope
3. Aspect
4. Profile curvature
5. Planar curvature
6. Longitudinal curvature
7. Cross-sectional curvature
8. Minimum curvature
9. Maximum curvature

The geomorphology of most landscapes is a mix of the primitive elements suggested by Wood (1996) and the basic classes suggested by Weiss (1991). The appropriate scale for analysing a particular landscape will, however, vary. To convert landscape mixes into well defined landform classes as done by, for example. Ballantine *et al.* (2005), requires a pre-defined set of classes. This last step can only be achieved with local knowledge and by including specific lithological classes. In general, landform maps are very scale dependent. Global geomorphological maps are small scale and show only large features, such as plains, mountains, sedimentary basins, peninsulas, etc. Hence, most global geomorphological maps are not useful for mapping features like wetlands.

As part of this study, an attempt was made to develop a global geomorphological map for assisting in mapping wetlands and wetland types. The map was developed using the SRTM DEM with a 250 m

Table 1. Simplified scheme of the principal rules applied for mapping global landform elements

Rule for	Input layer	General rule structure
Lakes and shores	MOD13Q1 Quality	If *Quality* = q
Rivers	TPI_x GTWI $CPROF_x$	If TPI_x < tpi & *GTWI* > w & $CPROF_x$ < c
Valleys	TPI_x $CPROF_x$ $slope_x$	If TPI_x < 0 & $CPROF_x$ < 0 & $CPROF_{x+1}$ < $CPROF_x$ & $slope_x$ < 1
	TPI_x $CPROF_x$ $slope_x$	If TPI_x < tpi & TPI_{x+1} < tpi & $PROF_{x+1}$ <= 0 & $slope_x$ < 1
Domes and alluvial fans	TPI_x $CPROF_x$ $slope_x$	If $CPROF_x$ >= 0 & $CPROF_{x+1}$ > $CPROF_x$ & tpi_a < TPI_x < tpi_b & $slope_{x+1}$ < 0.3
Mountains and ridges	TPI_x $CPROF_x$	if $CPROF_x$ > c & $CPROF_{x+1}$ > c & TPI_x > tpi
Steep slopes	TPI_x $CPROF_x$ $slope_x$	if $CPROF_x$ > c & $CPROF_{x+1}$ > c & TPI_{x+1} > tpi & ($slope_x$ > 15 or $slope_{x+1}$ > 15)
Plains	TPI_x $CPROF_x$ $slope_x$	if -c <= $CPROF_x$ <= c & -c <= $CPROF_{x+1}$ <= c & TPI_x <= 0 & $slope_x$ < 1
	TPI_x $slope_x$	if -tpi <= TPI_x <= tpi & -tpi <= TPI_{x-1} <= tpi & $slope_x$ < 10

TPI – topographic position index; CPROF – curvature profile; GTWI – global topographic wetness index.

Rules (except for lakes and shores) were applied to the hierarchy of scales (x) of the respective indices generated from five different scales of the original DEM used in the analysis (see text).

spatial resolution. The SRTM DEM was re-sampled (bilinear interpolation) to four coarser resolutions – 750 m, 1500 m, 3000 m and 6000 m. The geomorphological classification was then undertaken using the original scale (250 m) in conjunction with these hierarchical scales. For each scale a set of geomorphological indices were generated as defined by Wood (1996) and Weiss (2001):

1. Slope steepness
2. Profile curvature
3. TPI

For the original 250 m resolution, the following additional indices were used:

1. GTWI (as defined above)
2. Flow accumulation
3. Channel index

The channel index was specially developed to identify active rivers and streams. It uses the same approach as described for the GTWI, but disregards the local slope steepness, tan(B), and considers instead the TPI and curvature profile.

The geomorphological classification is based on a hierarchical set of IF … THEN … ELSE … rules, sequentially capturing landform elements that compose most landscapes. In general the rules were written to capture landscape elements ranging in size from 250 m up to 6 km. For each landform element the rules were applied at three or four scales. Table 1 summarises the principles used for identifying the global landforms.

For all landform elements, GTWI was used as a dichotomous post-classifier to divide the elements into either wet or dry. The global geomorphological map was generated at a spatial resolution of 250 m. Figures 26, 31 and 38 illustrate the geomorphological map.

5. Methods II – optical satellite image processing

Images from optical EOS have been widely used to map wetlands. As stated above, however, traditional statistical approaches relying on a large number of reference sites cannot be used for mapping global tropical wetlands. Instead a set of biophysically anchored indices relating to the distribution of wetlands were developed. Some of these indices have been developed by others and are accepted tools for land surface mapping. Other indices were developed as part of this study to allow the mapping of global tropical wetlands from satellite images.

5.1 Identifying spectral end-members

Pixels in satellite images of the earth's surface can either represent a homogenous surface, or represent a mixture of different surface elements. The higher the spatial resolution, the more likely it is that a pixel represents a single feature. In coarser images, pixels represent a mixture of different features. Identification of the spectral signal of a single feature in a satellite image enhances the interpretation of the satellite image. It is also a pre-requisite for attempting to un-mix the spectral signal into its components, or to remove the spectral signal from a particular feature.

In this study spectral end-members were identified for the MODIS MCD43A4 reflectance product (500 m spatial resolution, 7 bands) and for the MOD13Q1 vegetation product (250 m spatial resolution, 4 bands) separately. Routines were developed for automatic regional (tile-specific) identification of four spectral end-members – dark soil, light soil, dense vegetation and open water.

5.1.1 Background

In multi-spectral satellite images, such as images derived from the MODIS sensor, complete spectral un-mixing is inherently impossible unless ground reference data on spectral end-members is available. And, even then, attempting to partition the relative occurrence of different features within a cell is a non-tractable problem. If, however, the objective of spectral un-mixing is to reveal the spectral signal of a cell disregarding one (or more) well defined spectral end-members the problem is more tractable. The definitions of wetlands and peatlands are based on soil conditions. Sub-classification relate to botanical features. Wetlands do have strong geo-botanical relationships, and geo-botanical relationships can assist in mapping wetlands from satellite images. But such an approach demands (local) knowledge or reference sites for identifying the spectral signal of geo-botanical classes in the area to be classified. Mapping global wetlands from geo-botanical information is hence prohibitive as assembling global knowledge of geo-botanical classes, their spectral signals and their global spatial distribution is a daunting task. A more generic approach is necessary.

One generic approach is to extract the spectral signal after removing that part of the signal which is derived from the vegetation 'foreground' and to only retain the soil 'background' part. Vegetation un-mixing can be achieved using a vegetation index only. Crippen and Blom (2001) developed a pixel un-mixing algorithm for unveiling lithology based solely on a vegetation index. Their algorithm is based on the assumption that the 'background' is invariant vis-à-vis the foreground (i.e. that there are no geo-botanical effects). The algorithm for their 'forced invariance' pixel un-mixing is straightforward, but overlooks important background features. Because their algorithm is based solely on image data, it is a forward (or data) driven approach. In a goal driven approach (as in traditional pixel un-mixing) the end-members are *a priori* known. For a global approach, this is not possible, because of a lack of reference data and *a priori* knowledge of the distribution of wetlands and their spectral signals.

In this study, an alternative, forward driven pixel un-mixing algorithm based on eigenvectors representing different ground features was developed. One of the eigenvectors was set to represent vegetation, and removal of the vegetation from the spectral signal was done by reversing the eigenvector and reassembling the spectral signal while excluding vegetation. For this eigenvector spectral un-mixing approach to work, a set of spectral end-members must be defined in order to correctly identify the eigenvector for vegetation. A pre-requisite for spectrally removing the vegetation 'foreground' is identifying the spectral

signal of the vegetation end-member. Vegetation mapping from satellite images is very common, but not a trivial task. A variety of different approaches and algorithms have been suggested. A major obstacle in vegetation mapping is to correctly define and consider the background material – the soil line.

5.1.2 Defining vegetation density and the soil line

The classical index for extracting vegetation from satellite images is the normalised difference vegetation index (NDVI), defined as:

$$NDVI = \frac{(NIR - VIS)}{(NIR + VIS)}$$

where NIR is the reflection in the near-infrared, and VIS the reflection in the visible (usually red) wavelength. NDVI has been widely adopted for vegetation studies in remote sensing, and several improvements have been suggested, including the soil adjusted vegetation index (SAVI) (Huete 1988):

$$SAVI = \frac{(NIR - R)}{(NIR + R + L)}(1 + L)$$

where R is the reflection in the red wavelength, and L is a calibration (or noise) factor, usually set to 0.5.

Both NDVI and SAVI (and other vegetation indices derived from NDVI) assume that there is no vegetation when the visible/red reflection equals the near-infrared reflection. The soil background colour, however, influences the visible and near-infrared reflection differently. When the soil is not completely covered by vegetation it will affect primarily NDVI, but it also has an effect on SAVI (Baret and Guyot 1991). Lighter soils will influence the vegetation indices more than dark ones, and cause an over estimation of the vegetation cover. The problem with the classical vegetation indices is that the soil line is assumed to be the line where NIR = VIS. This is not the case. The soil line will vary dependent on soil conditions but, in general, it will not have an intercept at 0 and a unit slope. The concept of a generic soil line in remote sensing was proposed by (Richardson and Wiegand 1977):

$$NIR = \beta_1 R + \beta_0$$

where NIR is the near-infrared reflection, R is red reflection, β_1 is the soil line slope and β_0 the intercept.

Richardson and Wiegand (1977) also proposed the perpendicular vegetation index (PVI), calculated as the perpendicular distance of the cell's reflection in the NIR and R from the soil line. Clevers (1988) formulated a similar index for leaf area estimation – the weighted difference vegetation index (WDVI). Disregarding the soil line intercept, PVI/WDVI is defined as:

$$PVI = NIR - \beta_1 * R$$

And including the soil line intercept, the PVI is defined as:

$$PVI = (NIR - \beta_0) - \beta_1 * R$$

Hence the PVI is determined by first orienting the soil line in the R versus NIR space, and then measuring the Euclidean distance from the soil line to the reflection of NIR and R in this two-dimensional space. Mathematically PVI can also be expressed as a trigonometric function:

$$PVI = R * \sin\left(-atan\left(\beta_1\right)\right) + \left(NIR - \beta_0\right) * \cos\left(-atan\left(\beta_1\right)\right)$$

By using the trigonometric approach, the Euclidean distance parallel to β_1 can easily be calculated as a perpendicular background index (PBI):

$$PBI = R * \cos\left(-atan\left(\beta_1\right)\right) + \left(NIR - \beta_0\right) * \sin\left(-atan\left(\beta_1\right)\right)$$

The PBI is a useful index in itself, and also for analysing residual errors and non-linearities in the PVI.

Rondeaux *et al.* (1996) identified global values for the soil line, suggesting $\beta_0 = 0.0254$ and $\beta_1 = 1.086$, but the existence of such global values has been questioned. Baret *et al.* (1993) and Rondeaux *et al.* (1996) speculate that the lack of an accepted global soil line and difficulties in identifying the soil line in a satellite image with varying densities of vegetation have preserved the use of classical vegetation indices, despite their shortcomings.

5.1.3 Identifying regional spectral end-members

In this study, the global soil line, as defined by Rondeaux *et al.* (1996), was adopted as a starting point, and used for deriving PVI and PBI. Additionally, a global wetness index was defined from a linear band rotation, modelled on the widely accepted tasseled cap (TC) wetness component (Kauth and Thomas 1976):

For MCD43A4:

$$Wetness = B\,0.6885 + G\,0.1368 + R\,0.3741 + NIR\,0.1225 - MIR_a\,0.027 - MIR_b\,0.1768 - MIR_c\,0.5658$$

For MOD13Q1:

$$Wetness = B\,0.6885 + R\,0.3741 + NIR\,0.1225 - MIR_a\,0.027 - MIR_b\,0.1768 - MIR_c\,0.5658$$

where B is the blue reflection, G the green reflection, R the red reflection, NIR the near-infrared reflection, and the mid-infrared reflection (MIR) in the three MIR bands – MIR_a, MIR_b and MIR_c – of MODIS.

From the initial PVI, PBI and wetness indices, regional spectral end-members were identified. The routine suggested by Fox *et al.* (2004) was adopted for finding the soil line for each MODIS tile. The spectral search region was confined to PBI values falling on or near the global soil line and upper and lower limits were set for the PBI. The latter was done in order to exclude water saturated soils (at the PBI low end) and salt pans and bright beaches (at the PBI high end) from contributing to the regional soil line identification. To further minimise the influences of vegetation, the local (neighbourhood) variation in the PVI was used as a further constraint. Only if the standard deviation in the PVI of the surrounding pixels was lower than a given threshold did the pixel qualify as a spectral candidate for the soil line. This assures that the soil line is not contaminated by either water or vegetation, or by urban materials or other bright pixels. The soil line was identified from scenes representing a full annual cycle (i.e. 23 images). The reflection in all bands for the pixels recorded on or near the soil line was retained (not only NIR and R), as were the values for the PVI, PBI and wetness. The spectral end-members of dark and bright soils were identified from the high and low ends of the soil line. After the end points of the soil line had been identified, an expanding search box was applied until the 30 (or more) pixels falling closest to the end points had been identified. From these pixels the means and standard deviations of the reflections for dark and light soils were calculated for each band for each tile.

In order to identify the regional spectral end-members of dense vegetation and water, a simple search routine was applied to the PVI (vegetation) and wetness indices. For vegetation the search was constrained to a threshold in the PVI and local kernel variation (as described above). Dense vegetation was then defined from a minimum of 30 pixels representing the full annual cycle. The local spectral properties of water were identified in a similar manner, but using the wetness index as the search criteria (Figure 15).

The spectral end-members were used to define the spectral signals for dark soil, light soil, dense vegetation and surface water for each tile. Several studies emphasise the superiority of using local or regional soil lines for mapping biophysical properties from satellite images. The initial attempts to map global tropical wetlands were, therefore, undertaken using regional soil lines defined per tile. The variations in soil lines were, however, significant and, given the lack of local calibration data, a global soil line had to be defined and used.

5.1.4 Identifying global spectral end-members

For the 83 tiles composing the core global tropical region (vertical tiles in rows 7 to 10 in the MODIS tiling system), the spectral end-members for dark soil, light soil, dense vegetation and open water were used to identify global tropical spectral end-members. The definition of a global spectral end-member was achieved using a statistical Monte Carlo approach, constrained by both logical and empirical conditions. The constraints included:

1. Reflectance in all bands and all features >0
2. Dark soil reflecting less than bright soil in all bands
3. Vegetation highly reflective in NIR followed by MIR_a (short-wavelength infrared region – SWIR), and with low reflectance in all visible bands
4. Water showing a general decline in reflectance towards longer wavelengths
5. Eigenvector values for light soil all positive

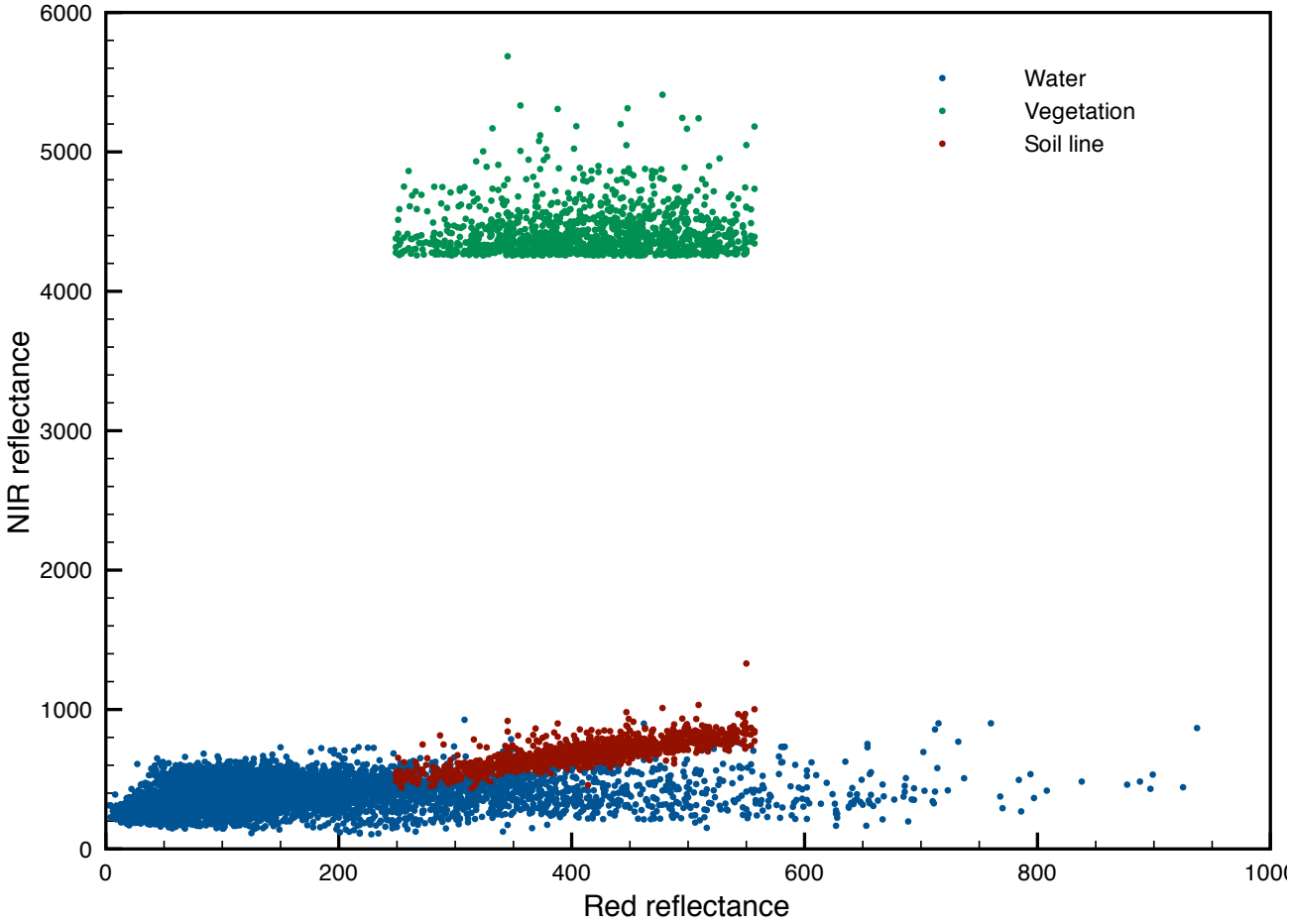

Figure 15. Spectral end-members extracted for tile h28v09 (parts of Sumatra and Java) The reflectance is multiplied by a factor of 10 000

Table 2. Mean and standard deviation (in parenthesis) for the ensemble of regional spectral end-members identified for tropical MODIS (MCD43A4) tiles (band order given as they appear in the MCD43A4 product

Material	R	NIR	B	G	MIR_a	MIR_b	MIR_c
Dark soil	0.0610	0.0985	0.0518	0.0631	0.1310	0.1249	0.0869
	(0.0208)	(0.0397)	(0.0220)	(0.0169)	(0.0676)	(0.0739)	(0.0556)
Light soil	0.1279	0.1674	0.0809	0.1099	0.2102	0.2213	0.1816
	(0.0292)	(0.0430)	(0.0226)	(0.0220)	(0.0746)	(0.0909)	(0.0797)
Vegetation	0.0493	0.4431	0.0296	0.0790	0.4040	0.2421	0.1013
	(0.0130)	(0.0425)	(0.0078)	(0.0124)	(0.0298)	(0.0209)	(0.0226)
Water	0.0290	0.0202	0.0386	0.0402	0.0198	0.0200	0.0135
	(0.0326)	(0.0158)	(0.0141)	(0.0283)	(0.0124)	(0.0105)	(0.0082)

6. Eigenvector values for vegetation highest in NIR followed by MIR_a (SWIR)
7. Eigenvector values for water declining with band wavelength.

Constraints 1, 2 and 5 are logical. The high reflectance of vegetation in NIR (constraints 3 and 6) is the basis for most classical vegetation indices, even though some use SWIR instead of NIR, as the SWIR reflection saturates at higher vegetation densities. The reflection of water is well established, with a general decline in reflectance from visible wavelengths, via NIR to MIR (constraints 4 and 7).

The spectral signal from each tile and for each feature was extracted to generate tropical ensemble means

Table 3. Global tropical spectral end-members (band order given as they appear in the MCD43A4 product)

Material	R	NIR	B	G	MIR_a	MIR_b	MIR_c
Dark soil	0.0656	0.0979	0.0423	0.0591	0.1221	0.1288	0.1177
Light soil	0.1262	0.1623	0.0858	0.1114	0.2163	0.2318	0.1337
Vegetation	0.0488	0.4847	0.0304	0.0807	0.4021	0.2428	0.0985
Water	0.0255	0.0188	0.0427	0.0359	0.0204	0.0206	0.0124

Table 4. Eigenvector values derived from global tropical spectral end-members, using dark soil as the offset factor (band order given as they appear in the MCD43A4 product)

Material	R	NIR	B	G	MIR_a	MIR_b	MIR_c
Light soil	0.337785	0.358966	0.242469	0.291520	0.525071	0.574122	0.089184
Vegetation	-0.384599	0.751599	-0.275617	-0.228412	0.279920	-0.244927	-0.143880
Water	0.083270	0.023793	0.341038	0.207347	-0.032848	-0.143196	-0.900897

and standard deviations (Table 2). The spectral signal for each feature and each band was randomised around the ensemble mean, allowing variations up to one standard deviation for each spectra (Table 1). The simulation was run until 30 successful spectral signals fulfilling the constraints had been generated (approximately 10 000 trials). The global spectral signal adopted was derived by taking the average spectral signal for each feature from the 30 successful simulations (Table 3). Applying an eigenvector transformation, using dark soil as the offset factor, the factors for each band for light soil (1st eigenvector), dense vegetation (2nd eigenvector) and open water (3rd eigenvector) are given in Table 4.

The derived eigenvectors were applied to produce both biophysical indices and for pixel un-mixing the reflectance, retaining only the reflectance of the background material.

5.2 MODIS linear data transformation to biophysical features

5.2.1 Background

PCA is a statistical technique for transforming n-dimensional vectors (i.e. image bands). The transformation is such that the information content is maximised in each sequential PCA component and each additional dimension is forced to lay perpendicular to the previous. PCA is applied in satellite image analysis to achieve a scene specific linear transformation. Applying the PCA transformation is comparatively easy; interpreting the results is much more difficult and includes studying the eigenvector values and visual inspection.

The TC transformation, first suggested by Kauth and Thomas (1976) for Landsat Multispectral Scanner data, is similar to a PCA, but with a fixed set of linear transformation values. The TC components were developed to represent intelligible biophysical properties – brightness, greenness, yellowness and 'other stuff'. Crist and Cicone (1984) developed TC components for Landsat thematic mapper (TM) data, expanding the original four components to six (brightness, greenness, wetness, yellowness and two biophysically undefined indices). Others have later developed TC transformations for satellite images acquired by a variety of sensors, including for MODIS (Lobser and Cohen 2007), Quickbird (Yarbrough *et al.* 2005) and CBERS-02B (Sheng *et al.* 2011).

When applied to reflectance corrected images, the TC transformation generates a consistent set of new, linearly transformed images. This is advantageous as the interpretation of the derived components is straightforward. At the same time, the information content is higher and more intuitive (Cohen *et al.* 2004). The TC components have been widely adopted for detecting change (Healey *et al.* 2005), and are reported to out-perform other methods for change detection.

5.2.2 Defining eigenvectors for biophysical transformations of MODIS images

A drawback of the original TC transformation is that it is based on 'top of the atmosphere' reflection. Thus, the derived components vary depending on atmospheric conditions. Adopting images corrected for atmospheric differences and variations in viewing angle, like the MCD43A4 product with reflectance corrected using a BRDF, overcomes this problem.

As mentioned above, this study initially attempted to use regionally (per tile) generated spectral end-members to define the eigenvectors to be used as components in a modified TC approach. This led to larger than expected variations in the definition of regional biophysical indices. Instead, the globally derived eigenvector values (Table 3) were adopted as component values in a modified TC transformation. In order to retain all the information in the original data, an additional set of default components were defined based on global spectral libraries (Table 5).

5.2.3 Transformations of MODIS images to biophysical indices

The eigenvectors derived from the identification of spectral end-members (Table 4) and the spectral end-members identified from spectral libraries (Table 5) were combined to create a TC-like transformation of MODIS reflectance data to biophysical indices. The reflectance of dark soil (Table 1) was used as an initial offset factor, and the remaining seven biophysical materials were then calculated using linear transformations:

$$BP_X = E_{Rx} R + E_{NIRx} NIR + E_{Bx} B + E_{Gx} G + E_{MIRax} MIRa + E_{MIRbx} MIR_b + E_{MIRcx} MIR_c$$

where BP is the biophysical material x, and E the eigenvector for the respective band and material x.

Apart from calculating the biophysical indices, the variation remaining after each successive transformation is also determined. The remaining variation after the last transformation is 0.

This modified TC transformation was applied to all tropical tiles.

5.3 Spectral un-mixing to reveal soil reflectance

5.3.1 Background

Pixel un-mixing is a widely used technique in many fields for retrieving the spectral response of a particular feature in a pixel that is a mixture of two or more features. The simplest case is a pixel which is a mixture of two materials (e.g. vegetation and water). With the spectral end-members of the mixture identified, it is straightforward to un-mix the reflection for the two materials. In many cases, however, more than two materials contribute to the absorbance (and hence the reflection) and the mixture might not be linear (one material might affect the absorbance of another). In a spectral un-mixing procedure, spectral end-members can either be inferred from laboratory derived reflection data (spectral libraries) or from end-members identified from the image itself.

Pixel un-mixing can more widely be divided into processes that are driven by the image data (forward or data driven) or by the *a priori* known spectral end-members (backward or goal driven). The most common approach is to use a backward driven approach and a linear un-mixing model. For the pixel un-mixing of soil versus vegetation this is not a trivial task. It is not trivial primarily because the soil reflection (along the soil line) means that there are at least three signature mixtures in each pixel, and the surface (and vegetation) moisture status adds further complication. The spectral properties of these materials do in fact interact and the un-mixing problem becomes non-linear.

5.3.2 Spectral un-mixing using eigenvectors

A major advantage with eigenvectors is that it is easy to reconstruct the original data by reversing the transformation. By excluding one or more of the transformed vectors, the reconstruction can eliminate specific information. In PCA this is normally done to compress the data and only retain the components carrying the most information, but it can also be used to exclude a component. For the MODIS image data this approach was used to reconstruct the reflectance of each pixel, leaving out the vegetation part of the spectral signal. Figure 16 shows the tropical regions at the peak of the dry season with the vegetation component of the spectral signal removed.

The map is created from the same data as contained in Figure 4, but with the vegetation part of the spectral signal removed using eigenvector based pixel un-mixing.

5.4 Wetness index derived from optical reflectance data

5.4.1 Background

Both wetlands and peatlands are characterised by wet conditions. The surface wetness is relatively higher as compared to other terrestrial soils; the groundwater table is near the soil surface, and annual flooding is common. The TC derived wetness component can

Table 5. Eigenvector values for additional biophysical materials – derived from global spectral libraries (band order given as they appear in the MCD43A4 product)

Material	R	NIR	B	G	MIR_a	MIR_b	MIR_c
Senescent vegetation	0.340846	-0.211939	0.004674	0.092003	0.592179	-0.679305	0.135234
Concrete	0.026100	0.404685	0.270465	0.596556	-0.430734	-0.341731	0.322810
Woody biomass	0.765950	0.307586	-0.117497	-0.438222	-0.326585	-0.065288	-0.044133
Quartz	-0.165876	0.048768	0.813608	-0.513293	0.044736	-0.085972	0.187847

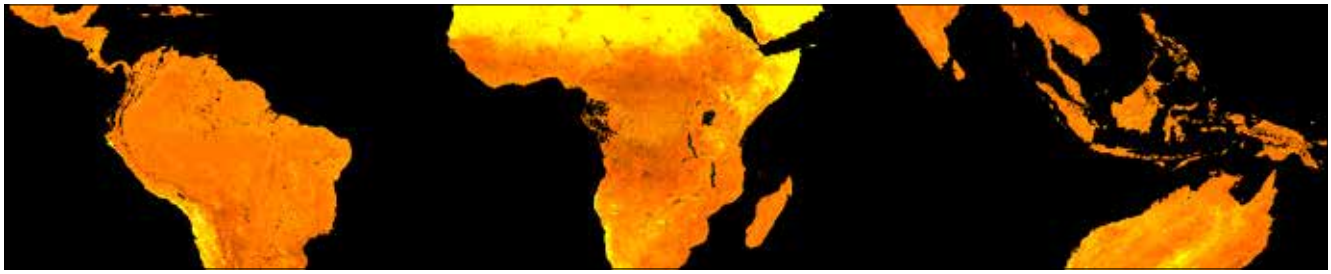

Figure 16. Colour composite of spectrally un-mixed MODIS tiles (peak dry season)

be used as a proxy for surface wetness (Nugroho *et al.* 2007). But most studies attempting to delineate wet areas use specifically designed wetness indices. McFeeters (1996) suggested a normalised difference wetness index (NDWI), analogous to the NDVI, for detecting water surfaces in Landsat (Enhanced) TM data:

$$NDWI = \frac{(G-NIR)}{(G+NIR)}$$

Rogers and Kearney (2004) suggested that the red band be used instead of the green and defined another NDWI as:

$$NDWI = \frac{(R-NIR)}{(R+NIR)}$$

Xu (2006) found inconsistencies in the NDWI using NIR as the reflective band as proposed by McFeeters (1996). Xu (2006) suggested exchanging NIR for a SWIR (SWIR equals MIR_a in the MODIS bands as used in this study) wavelength band, and thus defined the modified normalised difference wetness index (MNDWI):

$$MNDWI = \frac{(G-SWIR)}{(G+SWIR)}$$

Lacaux *et al.* (2007) suggested yet another wetness index, the normalised difference pond index (NDPI), for identifying small water bodies in West Africa:

$$NDPI = \frac{(SIR-G)}{(SWIR+G)}$$

Skakun *et al.* (2003) proposed the enhanced wetness difference image (EWDI), as the relative change in NDWI over two image dates. The EWDI approach has been adopted by others, mainly for studying vegetation phenology related to pest attacks (Coops *et al.* 2006).

Ji *et al.* (2009) compared the performance of the various versions of the NDWI listed above, and concluded that the combination of green and SWIR gave the most consistent results. Green was found to perform better than red. This is attributed to the difference in red reflection from the vegetation and the soil which is larger than the difference in the green reflection (see Table 2). The SWIR reflection is not saturated as quickly as NIR when vegetation cover increases and this is a probable reason why SWIR is better for use in wetness mapping than NIR.

Gao (1996) proposed another kind of NDWI, this one directed towards estimating leaf water content:

$$NDWI = \frac{(NIR - SWIR)}{(NIR + SWIR)}$$

The NDWI suggested by Gao (1996) has been widely adopted for studying vegetation phenology and vegetation change (Xiao *et al.* 2002; Maki *et al.* 2004; Wu *et al.* 2010). In some of the more recent studies it is called the land surface water index (LSWI). Its advantage over the classical normalised difference vegetation indices is that it saturates at a higher vegetation density.

The study on West African wetland by Landmann *et al.* (2010) used the LSWI (leaf wetness) phenology as a key information source for mapping wetlands.

5.4.2 A global wetness index derived from optical reflectance data

Most of the proposed wetness indices, except for the TC derived wetness, only use information from two spectral bands. The way the TC wetness is defined as an eigenvector retains some of the wetness in the two lower components (dark soil and vegetation), and the TC wetness index has thus not been extensively used.

In this study an alternative wetness index was developed. This novel index builds on the TC transformed components carrying information about soil brightness and wetness. Soil reflectance is largely dependent on mineral composition, carbon content and texture, but the water content is reported to be the major determinant of soil reflectance. As water strongly absorbs wavelengths in the visible, near and mid-infrared regions (cf. Tables 1 and 2), high water content equates to darker soil. Keeping this in mind, it is obvious why the TC wetness component is not optimal for mapping surface wetness. If it is assumed that dark soils (low values in the first TC component) have more water than light soils at the same wetness value, a more generic wetness index can be defined. This perpendicular wetness index (PWI) identifies a wetness line (analogous to the soil line) in the TC brightness versus TC wetness two-dimensional space (Figure 17).

Using a trial and error approach, different slopes and intercepts of the wetness line were tested and the results compared with the occurrence of wetlands in various tropical environments (mainly in Africa and South East Asia). The adopted PWI was re-defined as a trigonometric function:

$$PWI = TC1 * \sin\left(-atan\left(\beta_1\right)\right) + \left(TC3 - \beta_0\right) * \cos\left(-atan\left(\beta_1\right)\right)$$

By using the trigonometric approach, the Euclidean distance parallel to β_1 can be calculated as a second perpendicular background wetness index (PBWI):

$$PBWI = TC1 * \cos\left(-atan\left(\beta_1\right)\right) + \left(TC3 - \beta_0\right) * \sin\left(-atan\left(\beta_1\right)\right)$$

The intercept, β_0, was set to -2000 and the slope, β_1, to 0.6. The PBWI carries information that could potentially be used to identify non-linearities in the wetness line, but the lack of accurate and detailed ground data prevented testing for such non-linearities.

The PWI and PBWI were calculated for all the tropical tiles.

5.5 Wetness phenology

The occurrence and distribution of wetlands is, theoretically, directly related to the annual wetness phenology. The length of the periods of inundation and flooding are important, but the minimum, maximum and mean surface wetness also influence wetland formation and the accumulation of organic matter. Assuming that the definition of PWI is correct, open water will have a PWI value of 2200. Lack of reference data prevents an optimal definition of PWI for a completely inundated (but not flooded) soil. Other wetness conditions, like the PWI equivalent field capacity (soil wetness level at free drainage) or the wilting point, cannot be well defined. Instead, an arbitrary PWI level must be chosen to represent the wetness conditions needed for organic matter to accumulate. A preliminary PWI value of 500 was chosen to represent the wetness conditions necessary for peat formation.

The phenology of surface wetness, using a selected PWI value as an absolute threshold, should be a strong candidate for mapping global tropical wetlands. Prior to extracting the surface wetness phenology, the time series data of the PWI were used to fill no-data (i.e. cloud contaminated) dates with temporal interpolations using adjacent dates with valid PWI values. The interpolation was done as a

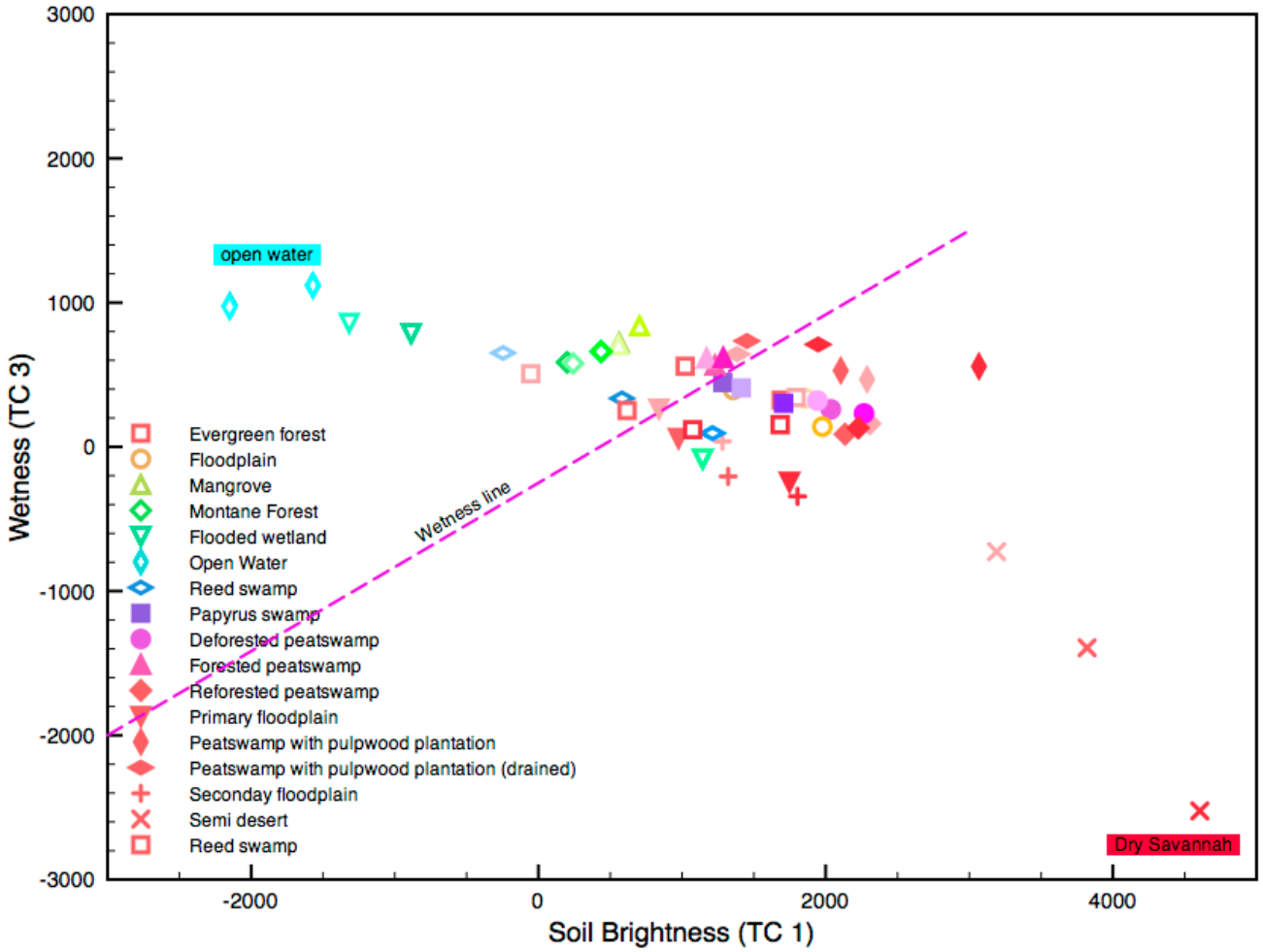

Figure 17. Theoretical construction of a generic wetness line in the two-dimensional space defined by the TC components for soil brightness (abscissa) and surface wetness (ordinate). Reference features are extracted to represent three phenological situations, end of wet season (most faded), peak dry season (intermediate) and end of dry season (un-faded)

weighted average, with the weights set according to the distances to adjacent dates with valid values. To account for no-data values at the start and end of the year, four dates prior to and post the annual cycle analysed were added. In this study 2011 was the year analysed and, hence, the last four dates in 2010 and the first four dates in 2012 were used when interpolating no-data values for 2011.

After filling the no-data points, a local regression algorithm was used to smooth the annual phenology cycle, with double weight put on data points derived directly from the PWI, as compared to data points derived by interpolation. The local regression was set to include seven dates in each regression. Figure 18 illustrates some of the phenological cycles representing various wetland types.

The surface wetness phenology was extracted from the filled and smoothed annual time series of the PWI using an arbitrary value of PWI = 500.

The following ten indices were calculated for each pixel at 500 m spatial resolution:

1. Minimum surface wetness (min)
2. Maximum surface wetness (max)
3. Mean surface wetness in wet period(s) (mean)
4. Date of maximum surface wetness or peak of wet season (pws)
5. Date of minimum surface wetness or peak of dry season (pds)
6. Number of wet (dry) seasons (nrpeaks)
7. Date of start of the wet season following the longest dry period (sws)
8. Date of the start of the dry season following the longest wet period (sds)

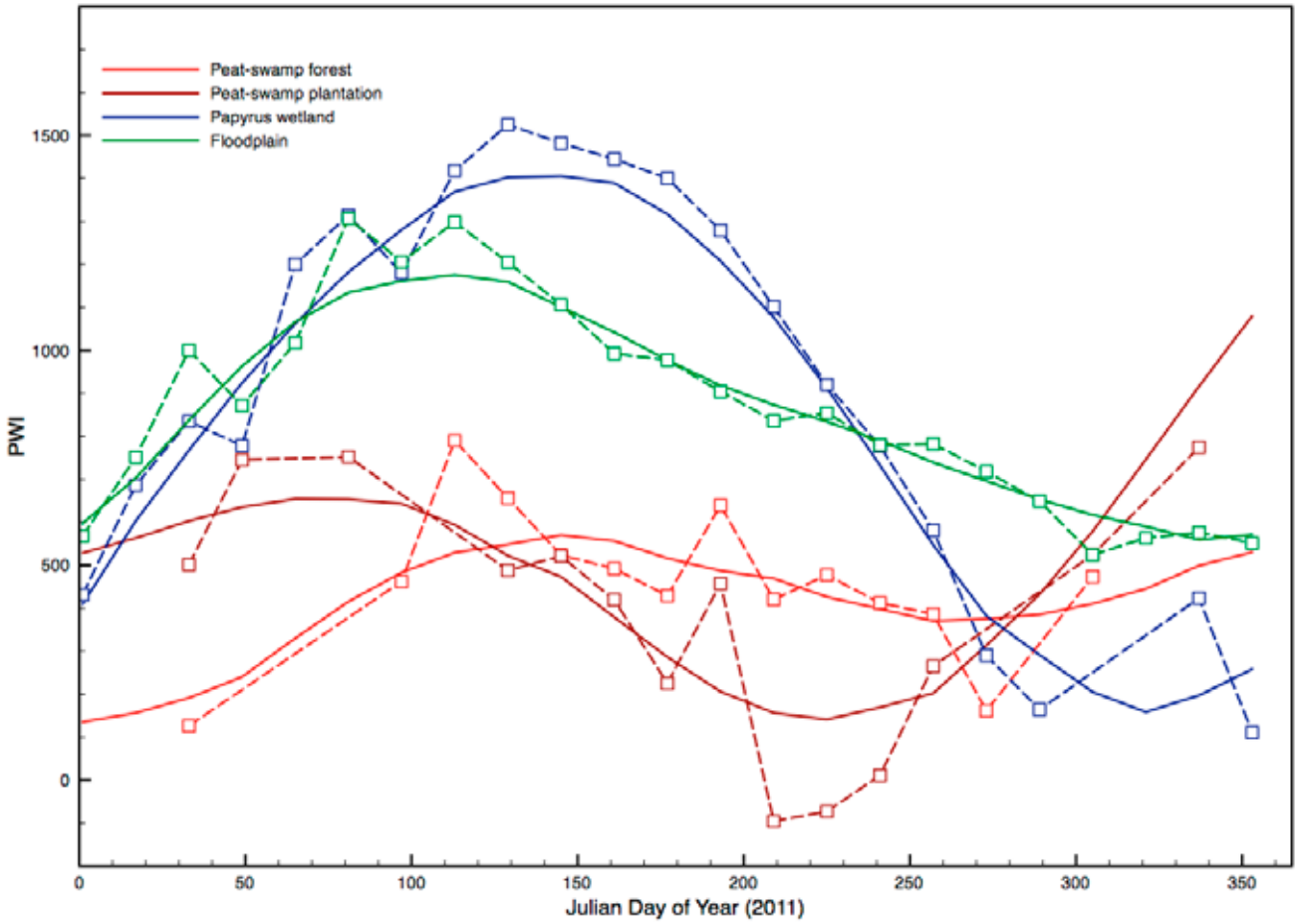

Figure 18. Phenological signals extracted from tropical wetland reference sites. Dotted lines represent the original index value and solid lines represent the index value after local regression smoothing

9. Length of the wet season(s) (lws)
10. Length of the flooding season(s) (lfs)

The indices extracted to describe the annual surface wetness phenology are similar to the phenological indices extracted for precipitation. The threshold for determining wet seasons and dry seasons was, however, set at a fixed PWI value and, additionally, a secondary threshold was set to determine flooding. Some of the phenological wetness indices are illustrated in Figures 19 to 23.

5.6 Spectral angle mapper (SAM) classification of global wetlands

The final wetland classification uses a chrono-sequence of images to extract phenologically relevant reference signals for use in image classification of defined spatial and temporal domains. The default spatial domain is defined in two ways. First by restriction to the MODIS tile in which the reference signal falls (neighbouring vertical and/or horizontal tiles can be included), and second, by restrictions imposed by the wetland likelihood map derived from wetness indices and the geomorphology. The temporal domain for a spectral signal is restricted by the local climate (precipitation) phenology. A reference signal can only be adopted for classification of a particular pixel if that pixel is in the same phase of the climate phenology as the reference site. Adopting a phenological similarity approach reduces the number of images to be analysed for an annual time series. The first results, reported here, are based on three phenological phases – the start of the dry season, the peak of the dry season and the start of the wet season.

The classification can be done using any classification technique but, for this study, the SAM technique (Yuhas *et al.* 1992) was adopted. The classification can be done using any of the available data sets,

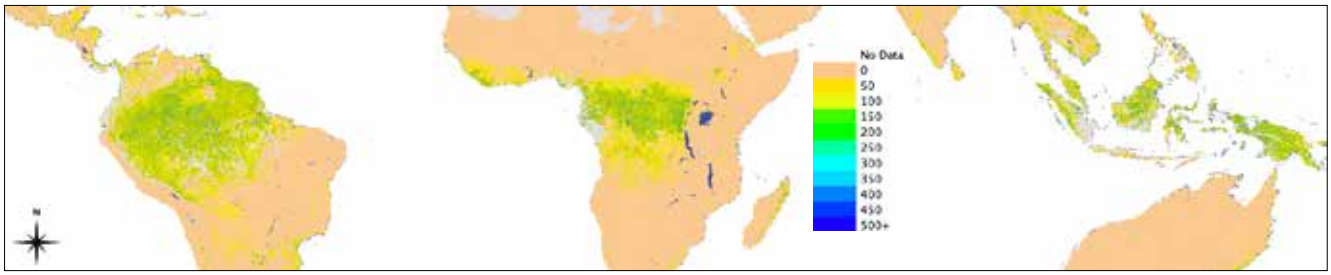

Figure 19. Minimum wetness index for 2011. Regions of minimum wetness most likely do not harbour any wetlands

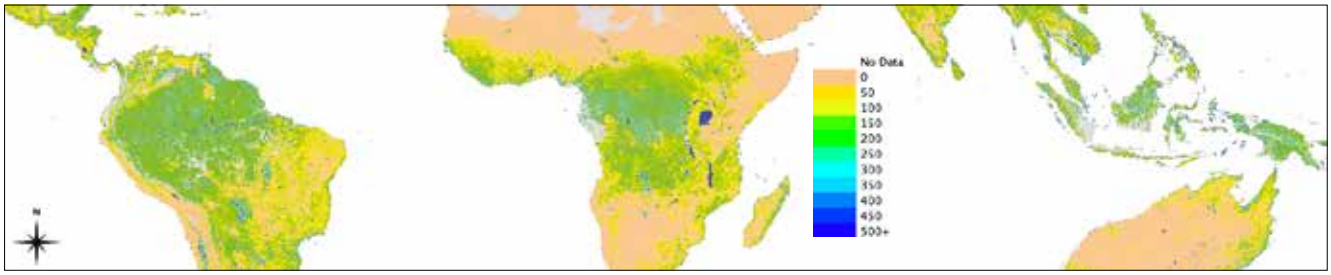

Figure 20. Maximum wetness index for 2011. Areas of maximum wetness below some (unknown) limit most likely do not harbour any wetlands

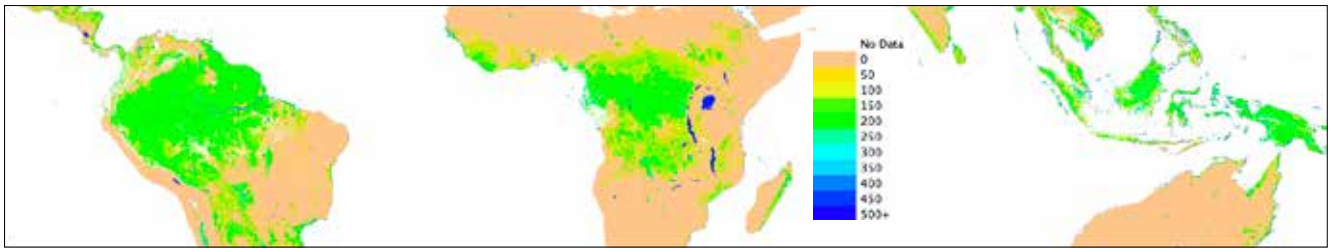

Figure 21. Mean wetness index for wet season(s) 2011 (see text)

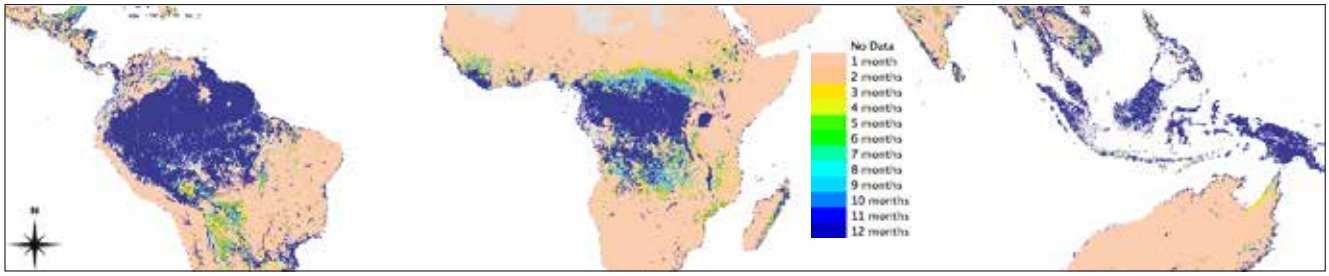

Figure 22. Length of inundation period(s) derived from the wetness index (see text)

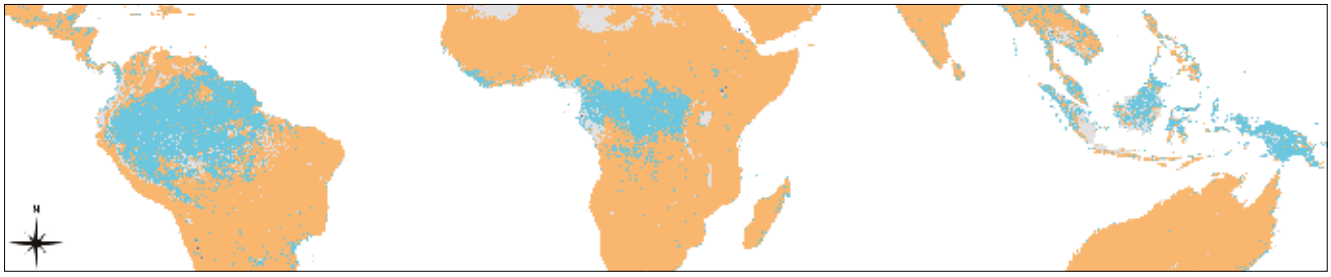

Figure 23. Areas of surface flooding in 2011 (turquoise) derived from the wetness index (see text)

including BRDF reflection, linearly transformed data, pixel un-mixed reflection, or phenology derived wetness of vegetation.

SAM compares the angles formed between reference spectra and the image spectra, treating them as vectors in n-dimensional space.

$$\alpha = \cos^{-1} \frac{\Sigma XY}{\sqrt{\Sigma X^2 \, \Sigma Y^2}}$$

SAM has some advantages over traditional statistical classifiers, like maximum likelihood. It is less sensitive to shadow effects and scan line edge effects. For most optical sensors the latter are minor problems (even less so for the BRDF corrected MODIS reflectance products). For radar data with a higher incidence angle, the weaker scatter returned from objects further away can still be classified with SAM, but not with a traditional classifier. SAM also has some drawbacks, mainly that positive and negative changes in spectral signals are not separated.

In the classification stage, reference data is used to identify similar areas in the spatial and temporal domain defining its validity. Lack of reference locations for large parts of the global tropics has, hitherto, prevented development of a full global tropical wetland map. As the mapping procedure is fully automated, the global tropical wetland map will be completed as soon as reference sites covering the tropics have been assembled and verified.

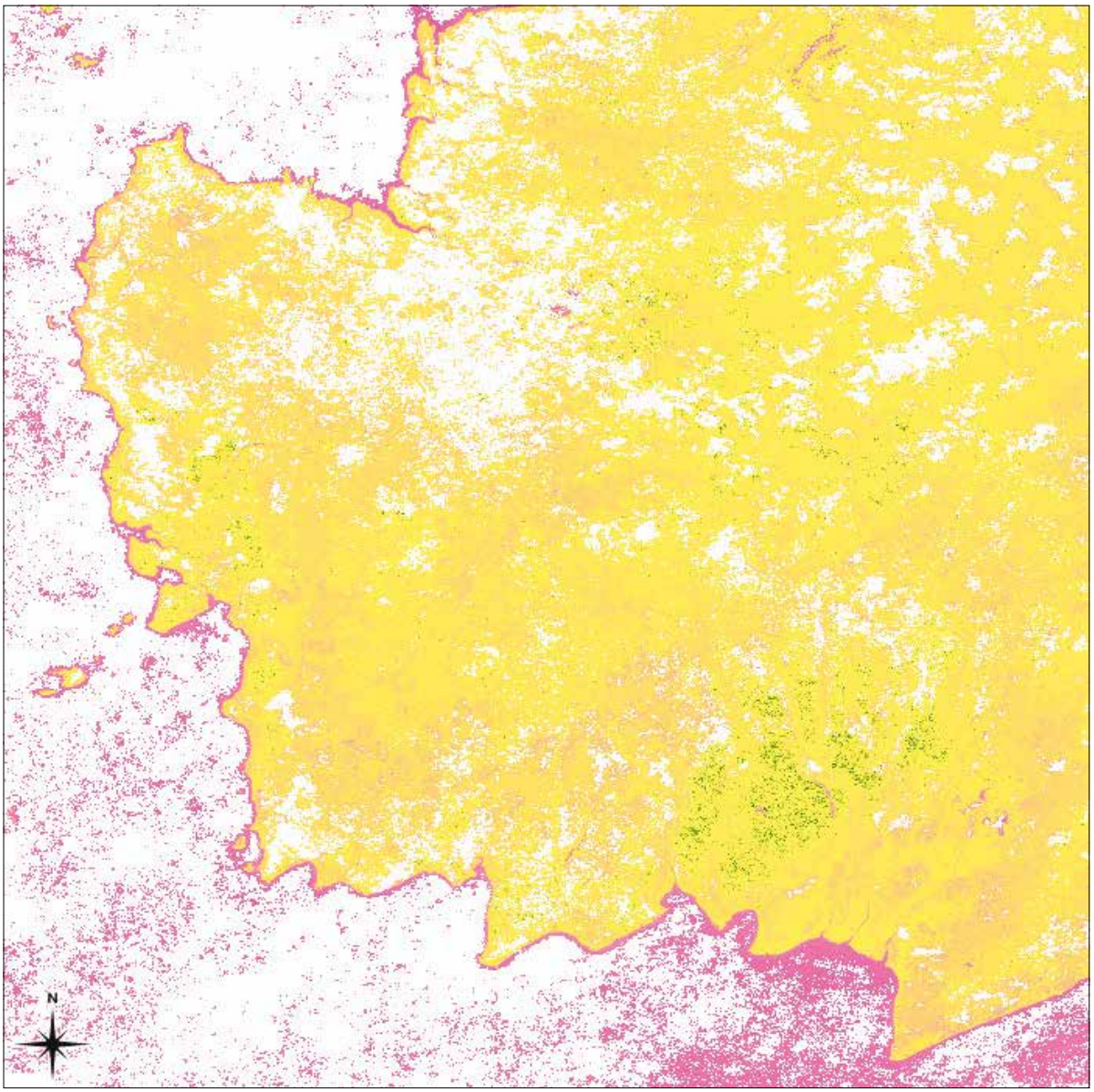

Figure 24. SAM classification of peat swamps in Kalimantan (Indonesia). Green areas have the most peatland, followed by yellow and purple. The reference data is captured from very small scale maps and is not verified. The classification represents a single date

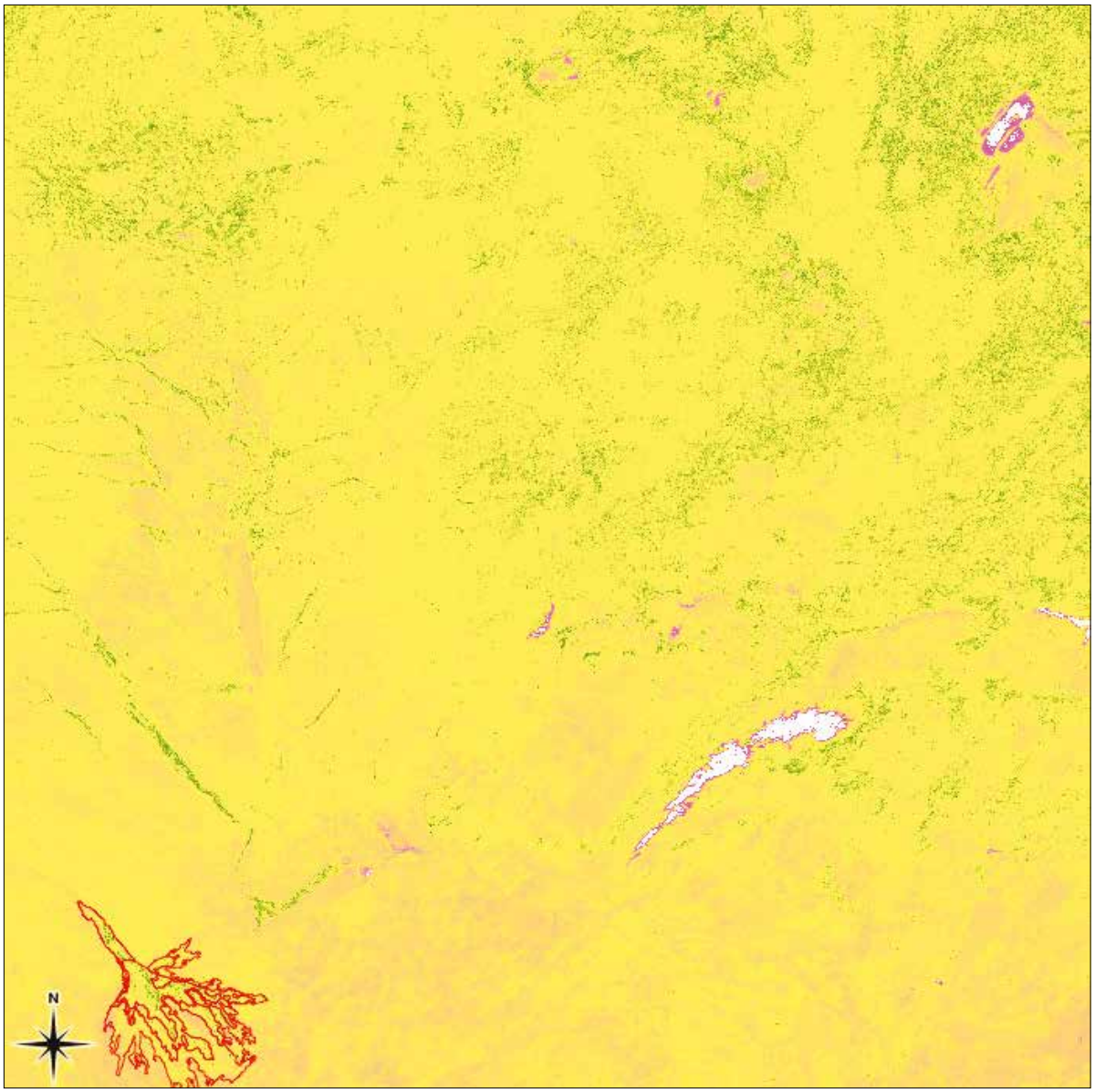

Figure 25. SAM classification of flood plains for tile h20v10 (Angola, Botswana, Namibia, Zambia and Zimbabwe). The Okavango Delta (Botswana) is outlined in red (lower left corner). Green areas have the most area in the flood plain class, followed by yellow and purple. The reference data is not verified. The classification represents a single date

6. Topography and peat depth

6.1 Topographic landforms and wetland depth

The largest tropical wetlands by volume are ombrogenic peat domes (the dominating wetland type of South East Asia). These wetlands contain approximately half the total peat volume of the tropical wetlands. The spatially largest tropical wetlands are, as described above, bound to floodout rivers and alluvial fans in tectonically subsiding regions (mainly in Africa and South America). For these two types of wetlands – peat domes and floodout rivers – the depth (and volume) needs to be modelled from empirical relationships between flooding, wetness phenology and geomorphology as described below. Also, other wetlands (e.g. riparian wetlands, smaller flood plains and montane wetlands), need to be modelled using the same approach, but more empirical data need to be assembled before such an attempt can be made. For all models of wetland depth, a pre-requisite is that the wetland's spatial extent is known. Until reliable reference data for wetlands throughout the tropics has been assembled, and a final classification of tropical wetlands and their distribution has been achieved, the depth of tropical wetlands cannot, in general, be determined.

6.2 Ombrogenic peat domes

The ombrogenic peat domes of South East Asia evolved under very wet conditions. The formation of these peat domes usually depends on the presence of a lower layer of less permeable and water saturated peat soil (catotelm) and a thin and more permeable upper layer (acrotelm) (Hoyt *et al.* 2012). Low transmissivity of the catotelm retards water flow out of the dome and the peat rises above the surroundings. A few detailed and verified topographic surveys of peat domes have been published. Anderson (1964) presents nine profiles from coastal peat domes in Brunei and Sarawak. In trying to model these domes based on hydrology, vegetation and peat accumulation, Hoyt *et al.* (2012) concluded that the model formulations or the (hydraulic) parameters of peat domes had to be revised. It is difficult, at present, to estimate the depth of tropical peat domes from climatological and hydrological data alone.

The peat domes presented by Anderson (1964) rise between 3 m and 9 m above their surroundings, and have total depths varying from 3 m to 15 m. All typically have a central plateau, with steeper slopes towards the margins. The radii of the domes vary from about 2 km to 7 km. The accuracy of the topographic data (SRTM) available for this study

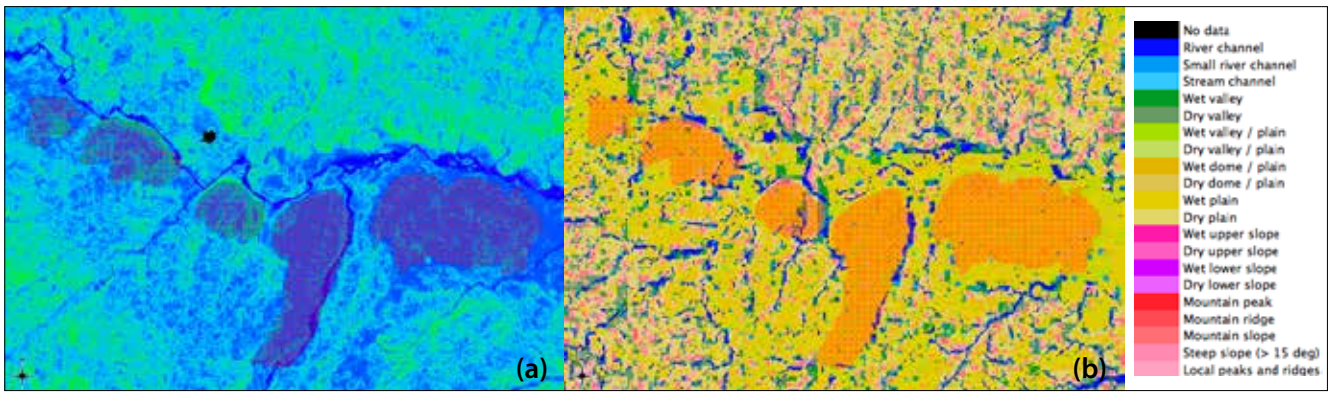

Figure 26. Details of five peat domes of varying size in Sumatra; a) GTWI and b) overlaying the global geomorphological map. The peat domes are associated with higher GTWI values (blue colours), but some blue areas are not associated with peat domes. The geomorphological map identifies the peat domes as wet plains, confined by channels, valleys or ridges. The accuracy of the peat map is not known

allows geomorphological characterisation of South Asian peat domes (Figure 24). The topographic data, however, does not have the accuracy required to delineate peat domes from other dome shaped (or near planar) surfaces. The well known subsidence of South East Asian peatlands following conversion to (oil palm) plantations, has led to changes in the geomorphology. This makes it more difficult to distinguish peatlands from other landscape features. The difficulty relates both to a loss in the originally typical landform (now more random) and in the drying out of the surface. Simultaneously, there has been a wide spread adoption of air and ground based remote sensing of the peat surface and peat depth. The data coverage for most of these studies is, however, marginal, often restricted to research sites or not available for public use.

6.3 Wetlands bound to floodout rivers and alluvial fans

The largest tropical wetlands are all bound to floodout rivers situated on alluvial fans between wet uplands and dry lowlands. The rivers feeding these wetlands also create the alluvial fans; the rivers meander back and forth and change direction by avulsion. As the distribution of water over the alluvial fans changes over time, the wetlands usually never accumulate more than a couple of metres of peat. Exceptions occur when tectonic subsidence is too great for avulsion to occur, as reported for the Pastaza-Maranon basin in Peru (Lähteenoja *et al.* 2012). In the Okavango Delta, Botswana, the rate of tectonic subsidence is slower. When the river changes its course, the peat which has accumulated will dry out and oxidate (Gumbricht *et al.* 2002). Hence, the peat in these extensive wetlands is not as deep as, for instance, in the peat domes of South East Asia. Gumbricht *et al.* (2005) developed a simple, but successful method for estimating the micro-topography of Okavango wetlands on an alluvial fan in Botswana. From empirical relationships between the wetland vegetation communities and the depth of flooding, they were able to accurately estimate the surface topography of the Okavango peatlands indirectly based on the levels of the underlying minerogenic sediments. Thus the approach used by Gumbricht *et al.* (2005) could be used to estimate the volumes of peat of the Okavango and similar wetlands.

7. Detailed analysis of peat domes and alluvial fans

For a few selected sites more detailed maps of wetlands have been assembled – including a peat map for Indonesia, and a wetland map of the Okavango Delta in Botswana (both with approximate scales of 1:250 000). In this section these two regions are used to illustrate the results of global mapping at a regional scale.

7.1 Indonesian peatlands

Indonesian peatlands cover approximately 200 000 km^2, or 10% of the Indonesian land surface. Figures 27 to 32 illustrate some of the global data sets presented and generated for southeast Kalimantan.

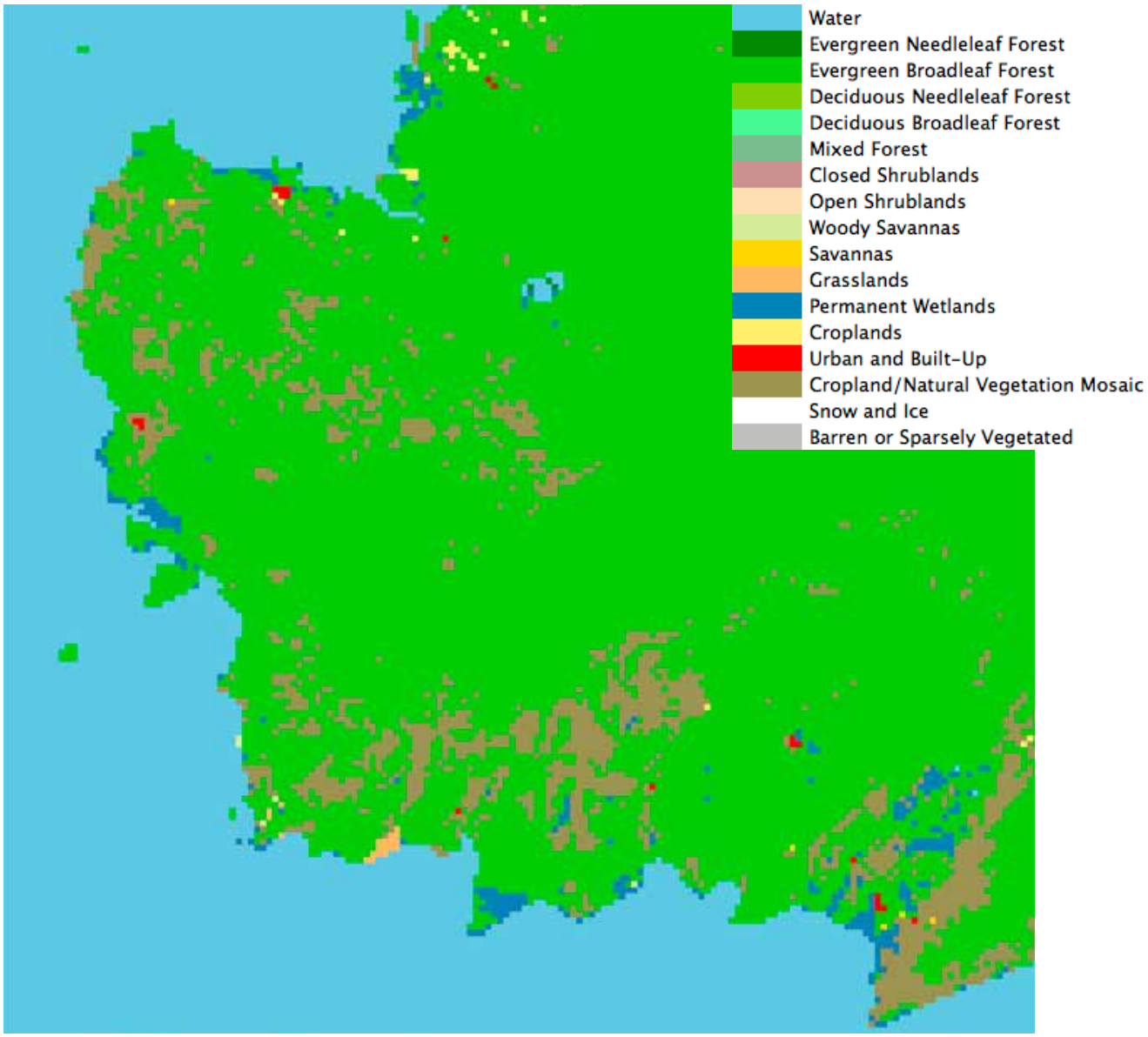

Figure 27. MODIS land cover (MCD12Q1) for southeast Kalimantan (Indonesia)

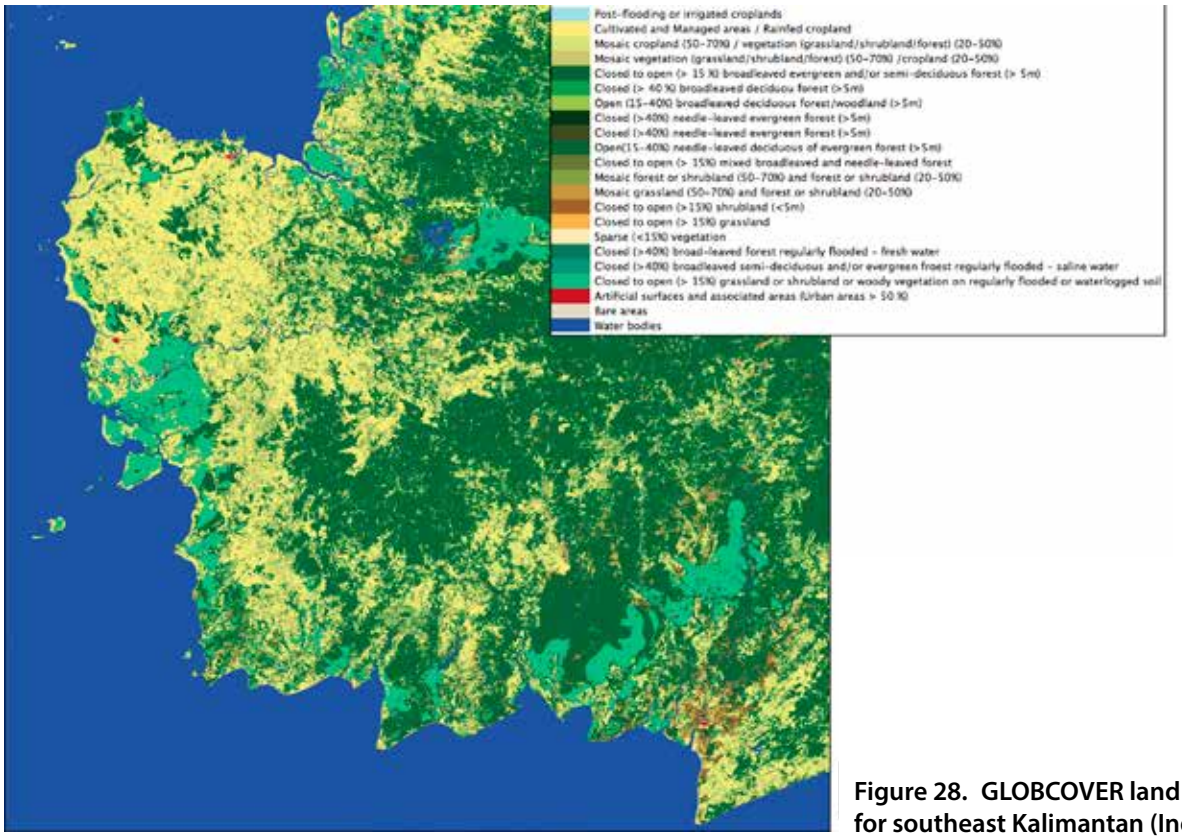

Figure 28. GLOBCOVER land cover (ESA) for southeast Kalimantan (Indonesia)

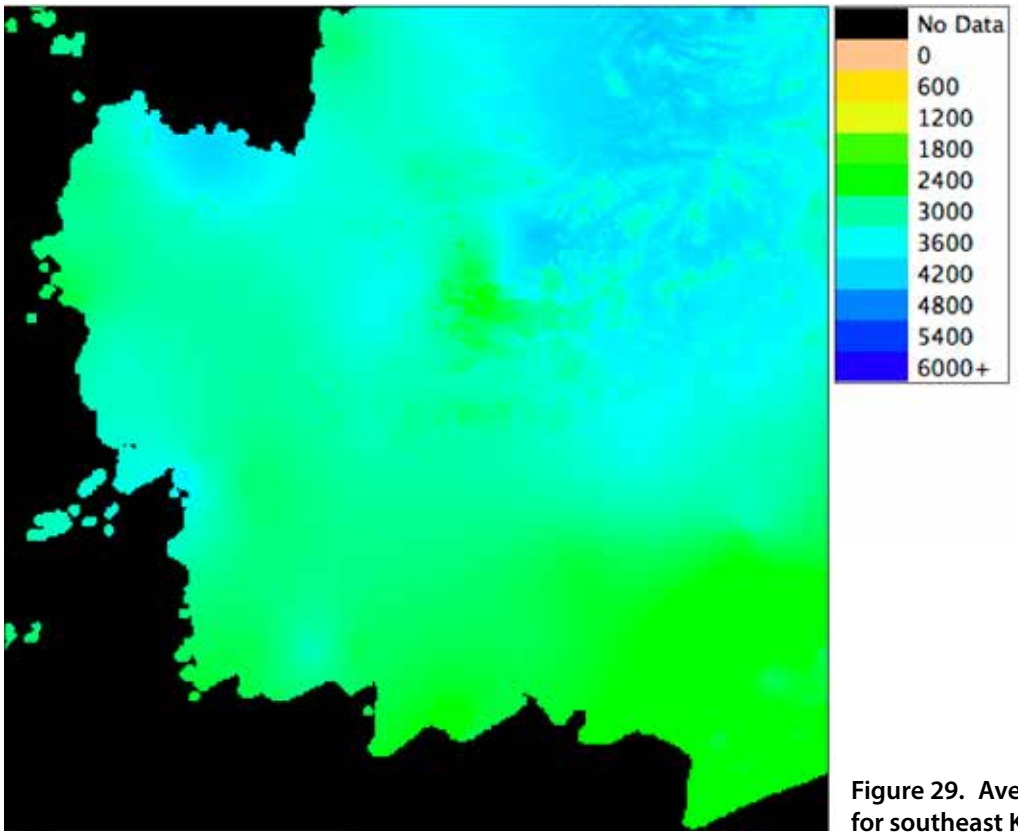

Figure 29. Average annual precipitation for southeast Kalimantan (Indonesia)

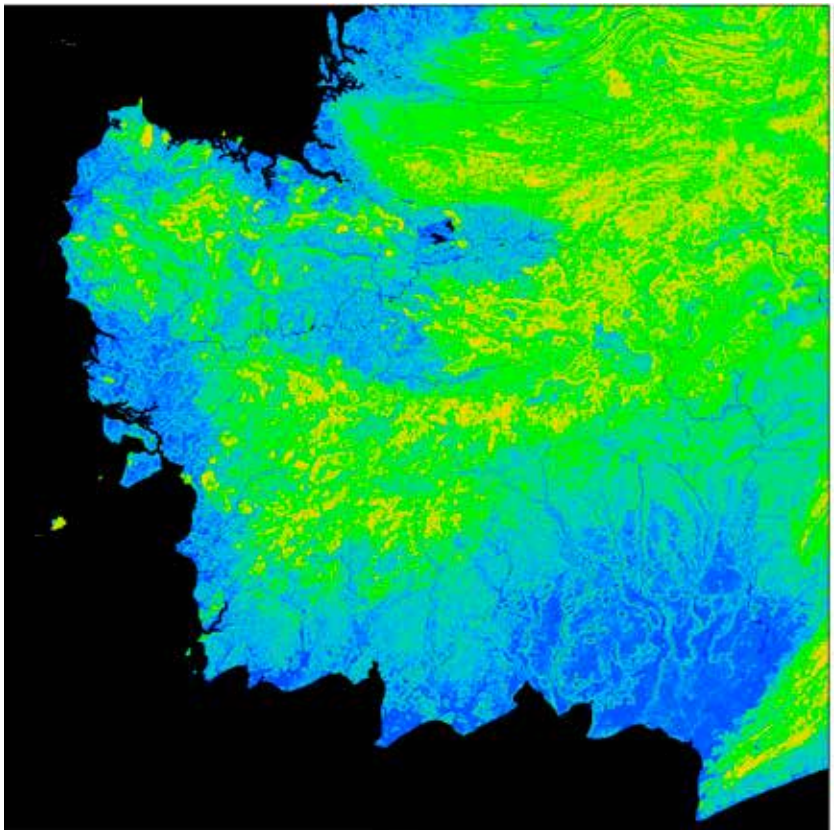

Figure 30. GTWI for southeast Kalimantan (Indonesia)

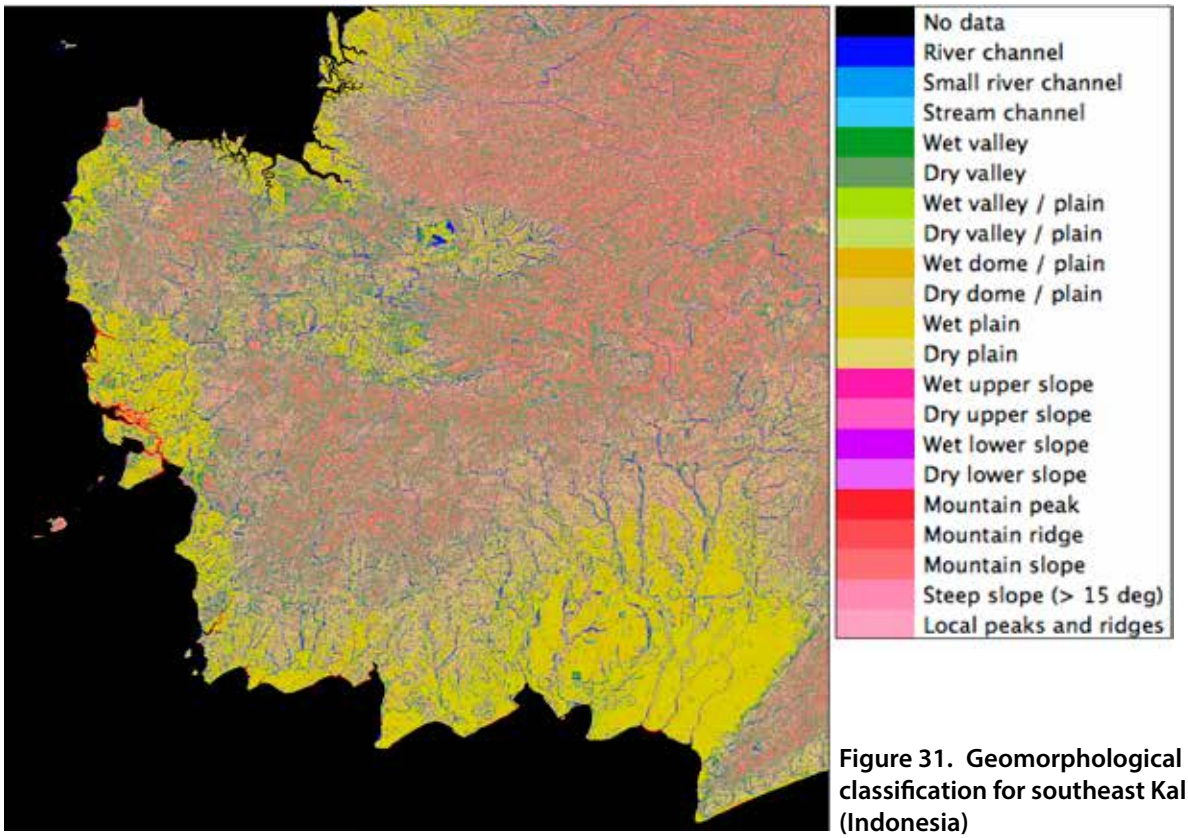

Figure 31. Geomorphological classification for southeast Kalimantan (Indonesia)

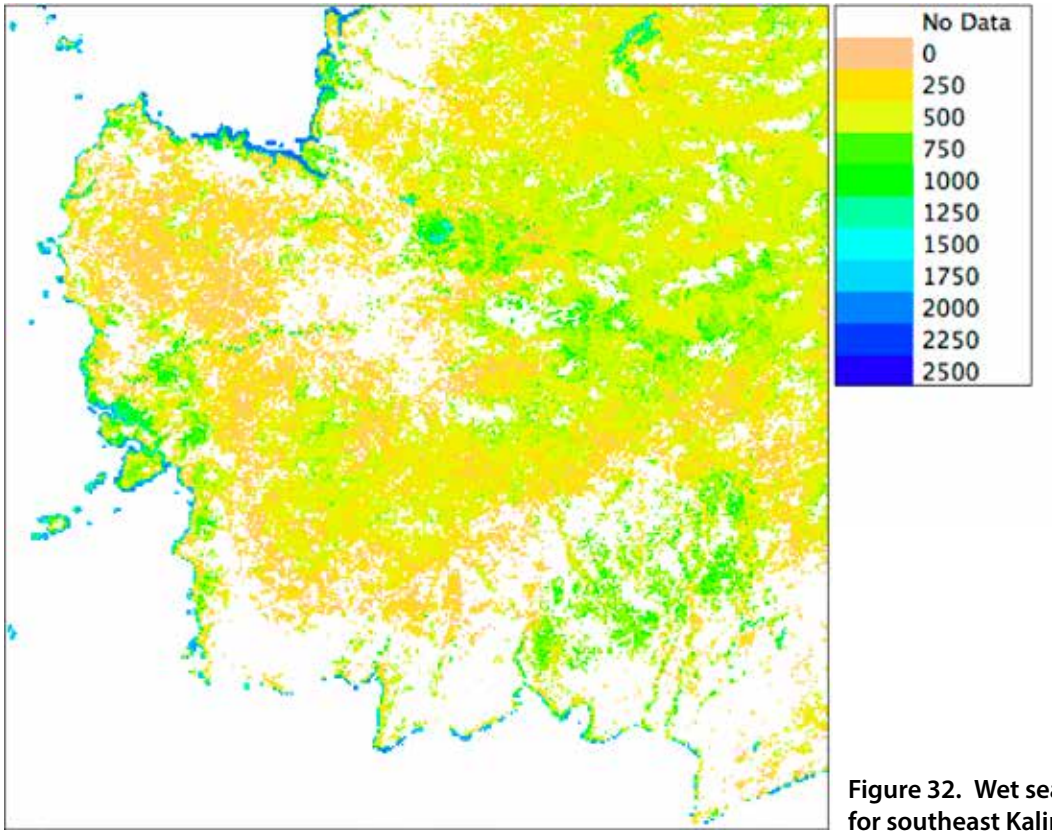

Figure 32. Wet season wetness (2011) for southeast Kalimantan (Indonesia)

7.2 Okavango Delta, Botswana

The Okavango inland delta in Botswana covers approximately 15 000 km^2, with peat accumulation covering approximately 9000 km^2. Figures 33 to 40 illustrate some of the global data sets presented and generated for the Okavango Delta in Botswana.

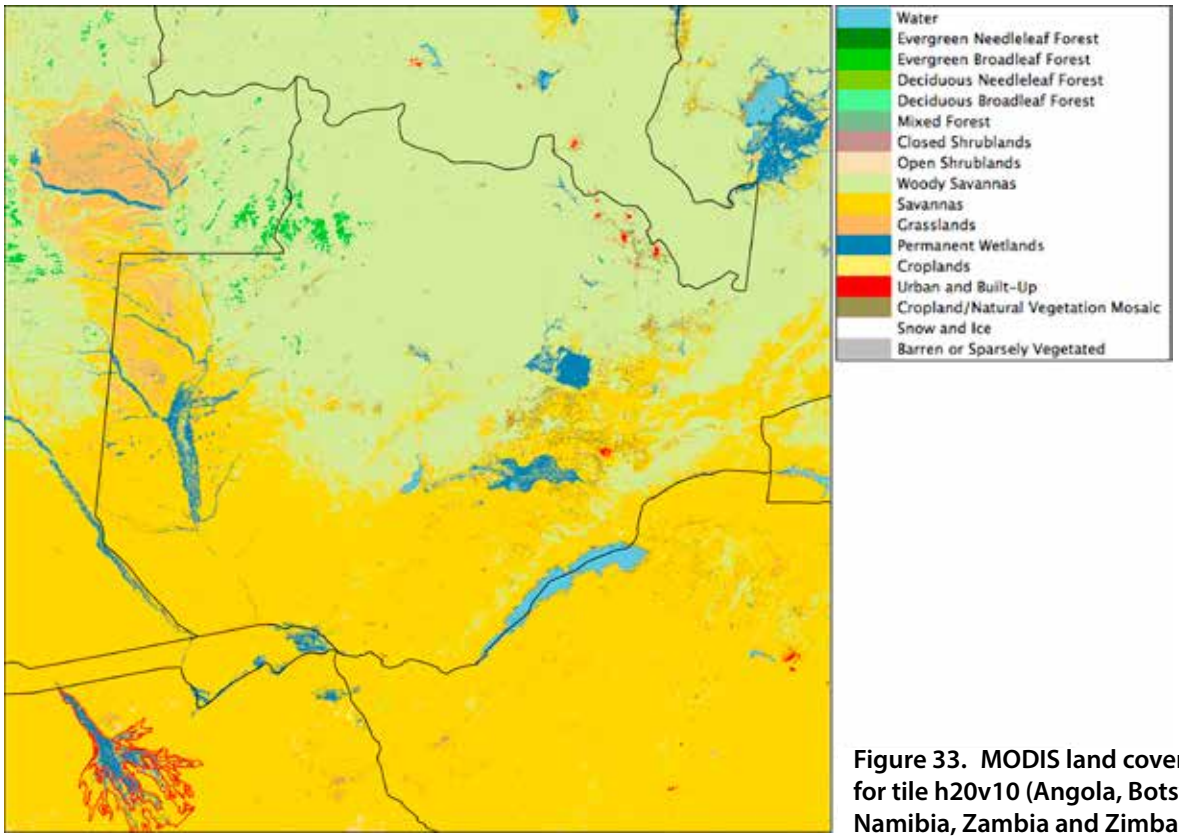

Figure 33. MODIS land cover (MCD12Q1) for tile h20v10 (Angola, Botswana, Namibia, Zambia and Zimbabwe)

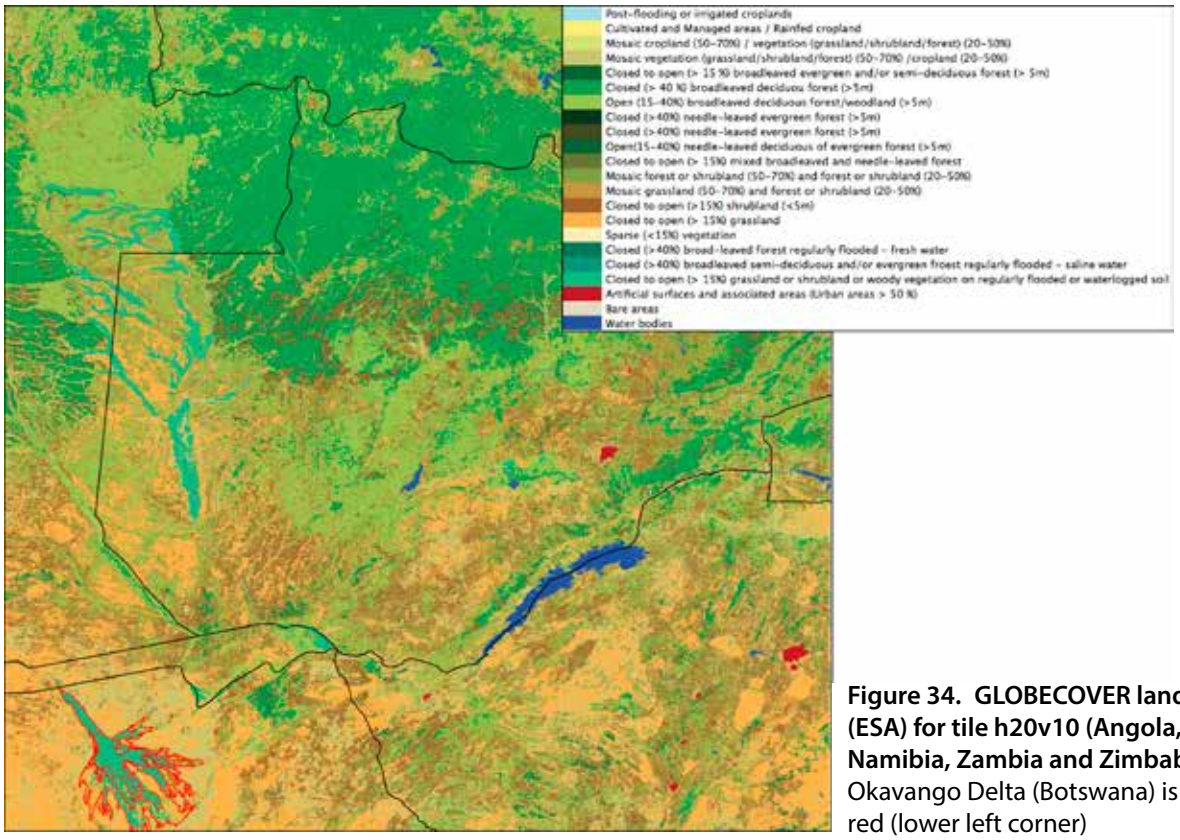

Figure 34. GLOBECOVER land cover (ESA) for tile h20v10 (Angola, Botswana, Namibia, Zambia and Zimbabwe). The Okavango Delta (Botswana) is outlined in red (lower left corner)

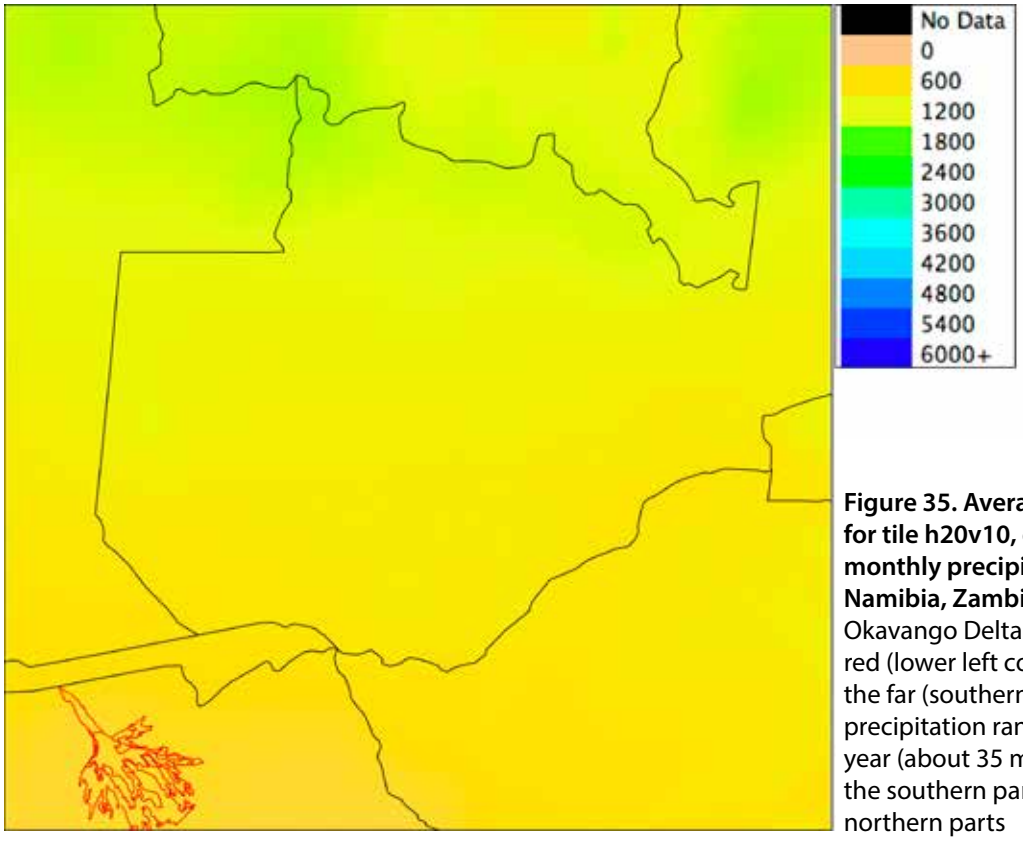

Figure 35. Average annual precipitation for tile h20v10, expressed as average monthly precipitation (Angola, Botswana, Namibia, Zambia and Zimbabwe). The Okavango Delta (Botswana) is outlined in red (lower left corner). The area represents the far (southern) end of the ITCZ, and precipitation ranges from about 400 mm/year (about 35 mm/month on average) in the southern parts to 1400 mm/year in the northern parts

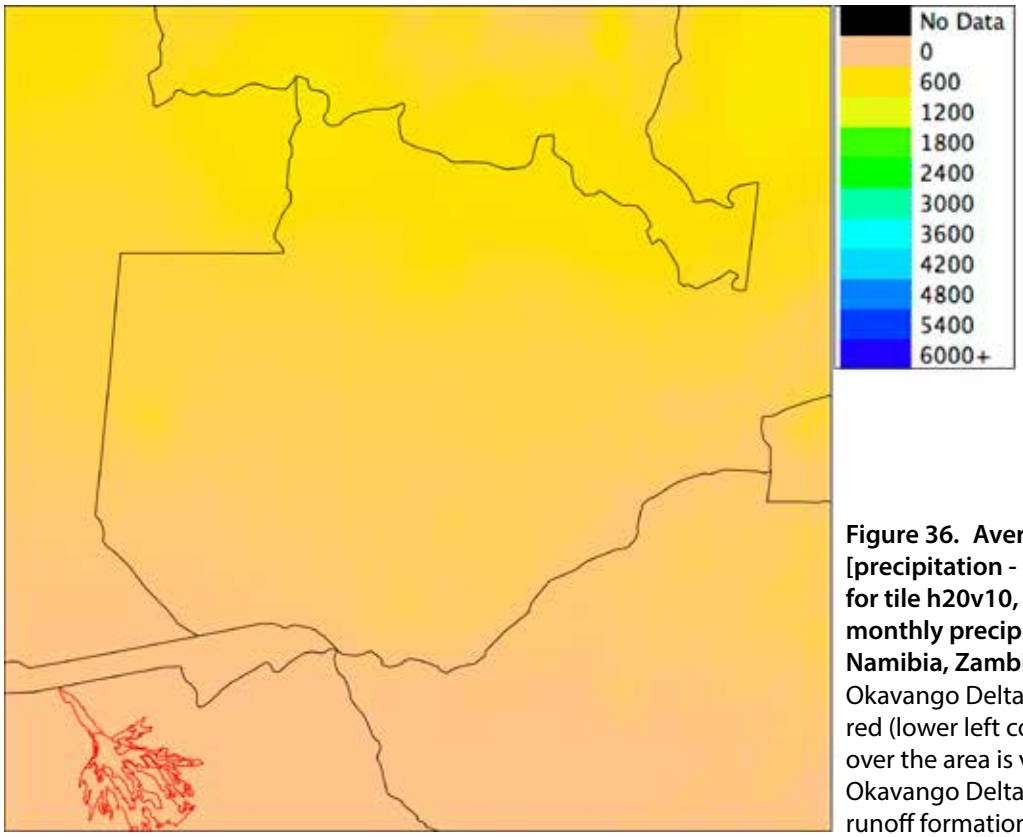

Figure 36. Average annual runoff rainfall [precipitation - evapotranspiration] for tile h20v10, expressed as average monthly precipitation (Angola, Botswana, Namibia, Zambia and Zimbabwe). The Okavango Delta (Botswana) is outlined in red (lower left corner). The rainfall runoff over the area is very low, and over the Okavango Delta there is no actual rainfall runoff formation

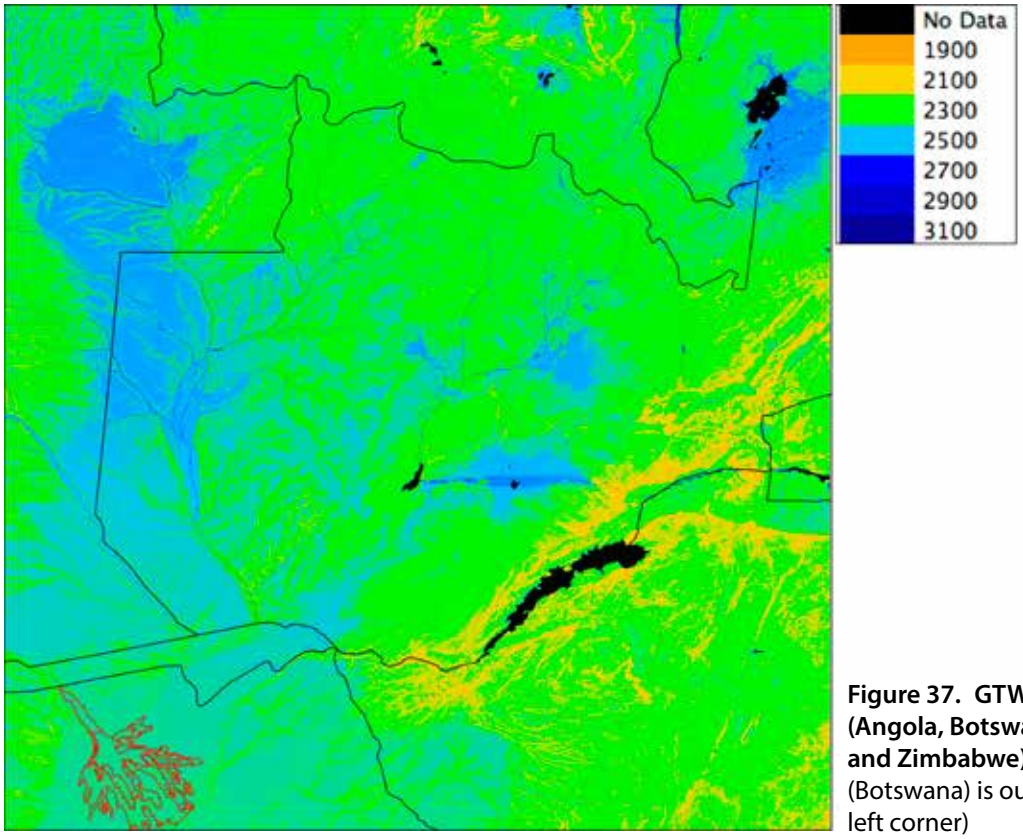

Figure 37. GTWI for tile h20v10 (Angola, Botswana, Namibia, Zambia and Zimbabwe). The Okavango Delta (Botswana) is outlined in red (lower left corner)

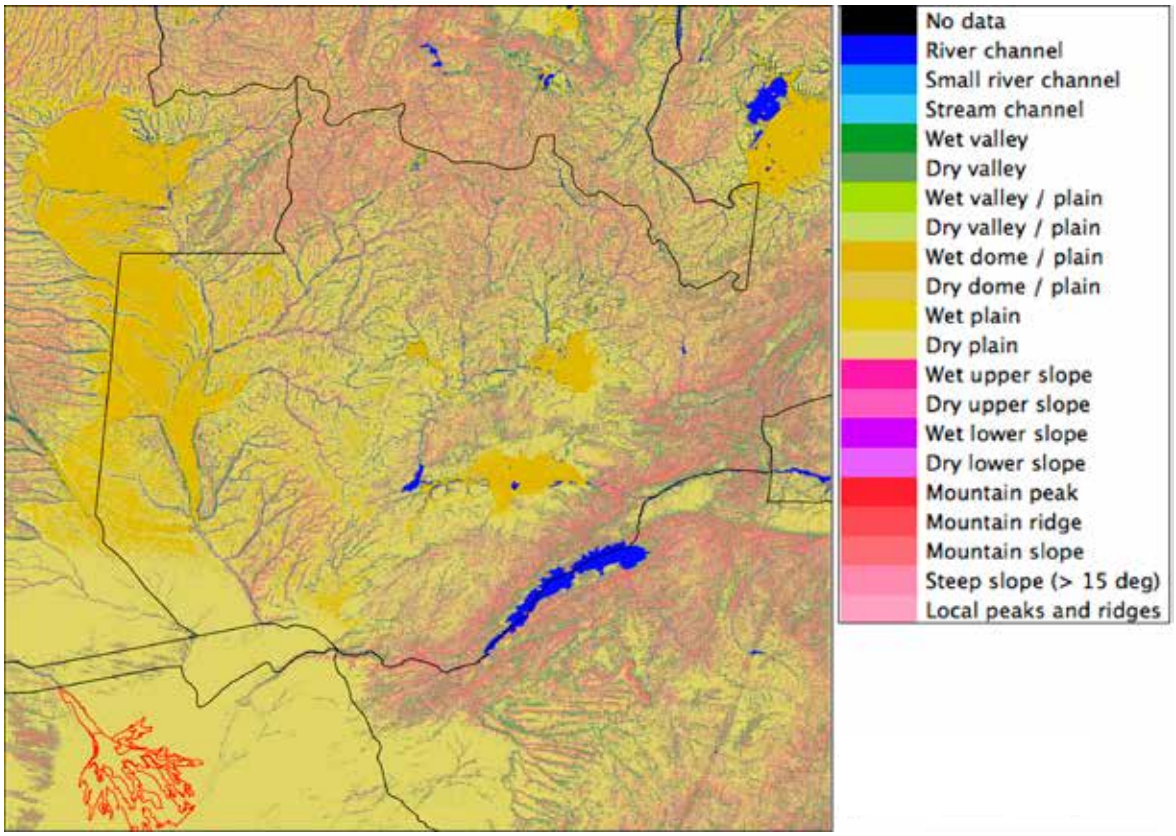

Figure 38. Geomorphological classification for tile h20v10 (Angola, Botswana, Namibia, Zambia and Zimbabwe). The Okavango Delta (Botswana) is outlined in red (lower left corner). The Okavango Delta is classified as a dry area – the DEM cannot resolve the flow accumulation over the Okavango as the data source (SRTM) is not accurate enough to portray the floodout of the Okavango River over the alluvial fan forming the foundation of the Okavango

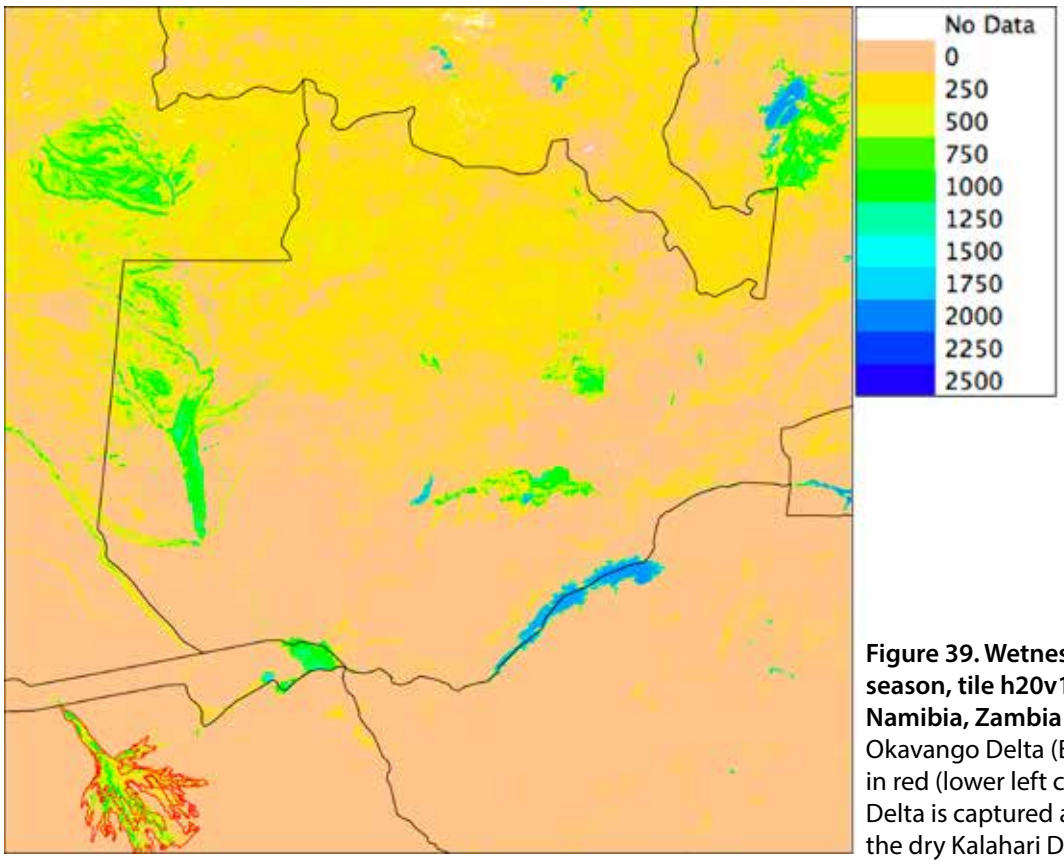

Figure 39. Wetness for the 2011 wet season, tile h20v10 (Angola, Botswana, Namibia, Zambia and Zimbabwe). The Okavango Delta (Botswana) is outlined in red (lower left corner). The Okavango Delta is captured as a wet environment in the dry Kalahari Desert

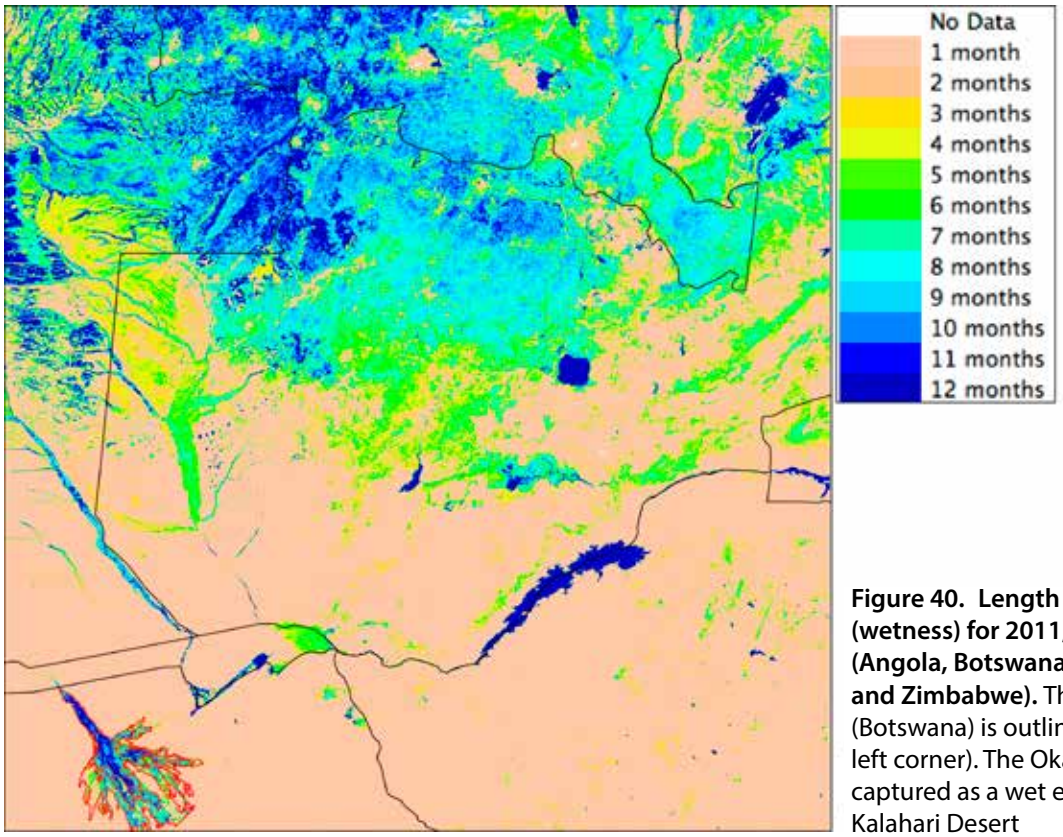

Figure 40. Length of wet season (wetness) for 2011, tile h20v10 (Angola, Botswana, Namibia, Zambia and Zimbabwe). The Okavango Delta (Botswana) is outlined in red (lower left corner). The Okavango Delta is captured as a wet environment in the dry Kalahari Desert

8. Conclusions

The extent, volume and carbon content of global tropical wetlands are not well known. The best estimates are based on disparate sources. Hitherto unknown wetlands are constantly being reported in the scientific literature. Traditional methods of classification, as well as more advanced methods adopted for global land cover (vegetation) mapping, are extremely difficult to adapt to mapping wetlands. The large variations in the appearance of wetlands, the typical fragmentary patterns of wetland soil and vegetation, and the variability of wetland flooding, inundation and vegetation phenology all contribute to the difficulty of mapping global tropical wetlands from EOS imagery. There is also a lack of adequate and verified ground reference sites for wetlands as compared with other classes of land cover. These problems prompted a novel approach to mapping global tropical wetlands, an approach which relies primarily on relevant biophysical indices that indirectly influence the distribution of wetlands. Existing indices on topographic wetness developed for temperate regions were reviewed and a novel GTWI was formulated. Optical multi-spectral image data was transformed into biophysical eigenvectors, in line with well established TC components. The eigenvectors were defined from global spectral end-members representing the global tropics. From the biophysical eigenvectors representing soil brightness and wetness, a novel surface wetness index was developed. Taking a full annual time series of this surface wetness index, the annual flooding and inundation phenology of the global tropics were estimated. The biophysical eigenvectors were also used for spectral un-mixing of vegetation and soil. This was done for a full annual time series of MODIS reflectance images (23 tiles/year) for the entire tropics. The soil spectral signal was used to test a chrono-sequence of automated SAM classifications of wetlands in regions with adequate reference data. The classification is stratified spatially and temporally, and the reference sites are used only for classifying wetlands in the same region and in corresponding climatic phenological phases. However, the reference data for these restricted regions (in Indonesia and Botswana) were not verified at a pixel scale.

Verified ground reference data is needed to test the potential of the classification scheme developed in this study. Existing data have only allowed visual comparison. A third wetness index was developed for radar (L-band) data, but the available global data set was plagued by positional errors that precluded its use.

8.1 Improving the global map of tropical wetlands

Several of the techniques and methods developed in this study have the potential to be improved and, hence, could lead to better predictions of the distribution of global tropical wetlands. Further development is hampered by the lack of verified (space and time relevant) ground reference data. Without such data none of the suggested improvements can be undertaken. Suggested improvements are listed in what is felt to be the order of importance and feasibility, beginning with the most important.

8.1.1 Definition of the PWI

The PWI was defined based on empirical assumptions and assuming a linear relationship between wetness and reflectance properties. The derived index was calibrated by visual inspection of its performance vis-à-vis comparatively well-mapped wetlands in Africa and South East Asia, and by analysing the PWI performance for theoretically pure and mixed spectral signals derived from spectral libraries. The parameterisation of the PWI is most probably not optimal, the biggest flaw being the non-linear relationship between surface wetness and vegetation leaf water content. Potentially, including a leaf water index and/or a non-linear definition accounting for non-linear mixing problems could improve the PWI significantly. A better definition of PWI will depend on the availability of time series data of surface (and leaf water) wetness. A number of such data sets are reported in the scientific literature, but none that are available in the public domain could be identified for this study (older data sets prior to the launch of the MODIS sensor do exist).

8.1.2 Inclusion of a (static) hydrological model

The GTWI developed as part of this study could be improved. Its major drawback is that local precipitation is used as a proxy for precipitation in

the drainage area. This is a gross oversimplification, especially in semi-arid and arid zones bordering the tropics where drainage areas reach into the tropics. To overcome this, a static hydrological model should be developed, accumulating not the drainage area but the rainfall runoff. The data needed for developing such a static model is included in this study and described above (apart from a DEM, only precipitation and evapotranspiration data are needed as inputs).

8.1.3 Access to better climate data sets

The WorldClim and FAO reference evapotranspiration data sets used in this study are statistical data sets. Hence, they do not reflect the ground situation for any particular year. The tropical rainfall measuring mission precipitation data set could be a better alternative for estimating rainfall. Better still would be access to national climate station data. Algorithms for estimating rainfall intensity and storm runoff could, potentially, also improve the mapping of global tropical wetlands.

8.1.4 Additional EOS data sources

It is well known that wetlands have elevated sensible heat fluxes (i.e. higher evapotranspiration) than adjacent land areas. Including a MODIS emissivity product could lead to better classification (mapping) of wetlands . Ideally emissivity data should be used to directly estimate evapotranspiration, using algorithms combining various MODIS and other climatic data sets.

8.1.5 Surface wetness mapping from advanced land observing satellite (ALOS) PALSAR data

Radar data from ALOS PALSAR has been made publicly available through the JAXA K&C initiative. This data was downloaded and organised as part of this study. Large errors in geometrical positions, however, precluded use of this data set. Attempts were made to write a pattern recognition algorithm to correct the geometrical errors, but the computational power needed to make satisfactory corrections was overwhelming. Improving the geometry of the PALSAR data sets would allow development of yet another, independent surface wetness index. The great advantage in developing such an index from radar data is that cloud has a negligible influence. Areas of the tropics with almost continuous cloud cover (parts of the Amazon and Congo Basins and parts of South East Asia) could be mapped with greater accuracy. The PALSAR data can also be used for independent image classification (e.g. the chrono-sequence SAM classification scheme) of wetlands using reference sites.

8.1.6 Stratification of mapping units

As described above, attempts were made to map regional soil and vegetation using the pre-defined MODIS tiles for stratifying the data. Spectral end-members were extracted for each tile and the spectral un-mixing was done using tile-specific data. This approach produced large variations and prevented definition of a tile-specific index (e.g. of the surface wetness index). Using the HWSD data (see Figure 1) to stratify the data based on soil classes (rather than tiles), should, in theory, improve both the definition of spectral end-members as well as improve the classification results from the SAM. However, the computational needs, as well as the needs for a substantially larger number of reference sites, are prohibitive.

9. References

Anderson, J.A.R. 1964 The structure and development of the peat swamps of Sarawak and Brunei. Journal of Tropical Geography 18: 8-16.

Arge, L., Chase, J.S., Halpin, P., Toma, L., Vitter, J.S., Urban, D. and Wickremesinghe, R. 2003. Flow computation on massive grid terrains. Geoinformatica 7(4): 283-313.

Bain, C., Bonn, A., Stoneman, R., Chapman, S., Coupar, A., Evans, M., Geary, B., Howat, M., Joosten, H., Keenleyside, C., Labadz, J., Lindsay, R., Littlewood, N., Lunt, P., Miller, C.J., Moxey, A., Orr, H., Reed, M., Smith, P., Swales, V., Thompson, D.B.A., Thompson, P.S., Van de Noort, R., Wilson, J.D. and Worrall, F. 2011 Commission of inquiry on UK peatlands. IUCN UK Peatland Programme, Edinburgh. http://www.iucn-uk-peatlandprogramme.org.

Ballantine, J., Okin, G., Prentiss, D. and Roberts, D. 2005 Mapping North African landforms using continental scale unmixing of MODIS imagery. Remote Sensing of Environment 97(4): 470-483.

Baret, F. and Guyot, G. 1991 Potentials and limits of vegetation indices for LAI and APAR assessment. Remote Sensing of Environment 35(2–3): 161-173. http://www.sciencedirect.com/science/article/pii/003442579190009U

Baret, F., Jacquemoud, S. and Hanocq, J.F. 1993. The soil line concept in remote sensing. Remote Sensing Reviews 7(1): 65-82.

Beven, K.J. and Kirkby, M.J. 1979 A physically based variable contributing area model of basin hydrology. Hydrological Sciences Bulletin 24(1): 43-69.

Bontemps, S., Defourny, P., Van Bogaert, E., Arino, O. and Kalogirou, V. 2010 GLOBCOVER 2009 Products description and validation report. MEDIAS-France, Toulouse, France. p. 27.

Brown, C.G., Sarabandi, K. and Pierce, L.E. 2005 Validation of the shuttle radar topography mission height data. IEEE Transactions on Geoscience and Remote Sensing 43(8): 1707-1715.

Bwangoy, J-R.B., Hansen, M.C., Roy, D.P., Grandi, G.D. and Justice, C.O. 2010 Wetland mapping in the Congo Basin using optical and radar remotely sensed data and derived topographical indices. Remote Sensing of Environment 114(1): 73-86.

Clements, T., Merriam, R.H., Stone, R.O., Eymann, J.L. and Reade, H.L. 1957 A study of desert surface conditions. Tech. Rep. EP-53. US Army Quartermaster. Research and Development Center, Environmental Protection Research Division, Natick, MA.

Clevers, J.G.P. W. 1988 The derivation of a simplified reflectance model for the estimation of leaf area index. Remote Sensing of Environment 25(1): 53-69. http://www.sciencedirect.com/science/article/pii/0034425788900417.

Cohen, W.B., Spies, T.A., Alig, R.J., Oetter, D.R., Maiersperger, T.K. and Fiorella, M. 2004 Characterizing 23 years (1972-95) of stand replacement disturbance in western Oregon forests with Landsat imagery. Ecosystems 5: 122-137.

Coops, N.C., Wulder, M.A. and White, J.C. 2006 Integrating remotely sensed and ancillary data sources to characterize a mountain pine beetle infestation. Remote Sensing of Environment 105: 83-97.

Costa, M., Telmer, K. and Evans, T. 2007 Seasonal dynamics of the Pantanal ecosystem. Phase 1 Report. JAXA EORC, Ibarati, Japan.

Cowardin, L.M., Carter, V., Golet, F. and LaRoe, E.T. 1979 Classification of wetlands and deepwater habitats of the United States. US Department of the Interior, Fish and Wildlife Service, Biological Services, Washington DC.

Crave, A. and Gascuel-Odoux, C. 1997 The influence of topography on time and space distribution of soil surface water content. Hydrological Processes 11(2), 203-210.

Crippen, R.E. and Blom, R.G. 2001 Unveiling the lithology of vegetated terrains in remotely sensed imagery. Photogrammetric Engineering and Remote Sensing 67(8): 935-943.

Crist, E.P.and Cicone, R.C. 1984 A physically-based transformation of thematic mapper data – the TM tasseled cap. IEEE Transactions on Geoscience and Remote Sensing 22: 256-263.

Curie, F., Gaillard, S., Ducharne, A. and Bendjoudi, H. 2007 Geomorphological methods to characterise wetlands at the scale of the Seine

watershed. The Science of the total environment 375(1-3): 59-68.Food and Agricultural Organization of the United Nations (FAO). 1998. World reference base for soil. World soil resources. Report No. 84. FAO, Rome.

Food and Agriculture Organization of the United Nations, International Institute for Applied Systems Analysis, International Soil Reference and Information Centre, Institute of Soil Science, Chinese Academy of Sciences and Joint Research Centre (FAO, IIASA, ISRIC, ISSCAS and JRC). 2012 Harmonized world soil database (version 1.2). FAO and IIASA, Rome, Italy and Laxenburg, Austria.

Fox, G.A., Sabbagh, G.J., Searcy, S.W. and Yang, C. 2004 An automated soil line identification routine for remotely sensed images. Soil Science Society of America Journal 68: 1326-1331.

Friedl, M.A., Sulla-Menashe, D., Tan, B., Schneider, A., Ramankutty, N., Sibley, A. and Huang, X. 2010 MODIS collection 5 global land cover: algorithm refinements and characterization of new datasets. Remote Sensing of Environment 114: 168-182.

Gao, B. 1996 NDWI—A normalized difference water index for remote sensing of vegetation liquid water from space. Remote Sensing of Environment 58(3): 257-266. http://www.sciencedirect.com/science/article/pii/S0034425796000673.

Gibbs, H.K., Ruesch, A.S., Achard, F., Clayton, M.K., Holmgren, P., Ramankutty, N. and Foley, J.A. 2010 Tropical forests were the primary sources of new agricultural land in the 1980s and 1990s. Proceedings of the National Academy of Sciences of the United States of America 107(38): 16732-7.

Giri, C., Ochieng, E., Tieszen, L.L., Zhu, Z., Singh, A., Loveland, T., Masek, J. and Duke, N. 2011 Status and distribution of mangrove forests of the world using earth observation satellite data. Global Ecology and Biogeography 20(1): 154–159.

Green, E., Clark, C., Mumby, P., Edwards, A.J. and Ellis, A.C. 1998 Remote sensing techniques for mangrove mapping. International Journal of Remote Sensing 19(5): 935-956.

Gumbricht, T., 1996 Modelling water and vegetation reciprocity - a landscape synthesis in GIS. Royal Institute of Technology, Division of Land and Water Resources. TRITA-AMI, PhD 1011, Thesis.

Gumbricht, T., McCarthy, T.S. and Bauer, P. 2005 The microtopography of the wetlands of the Okavango Delta, Botswana. Earth Surface Processes and Landforms 30: 27-39.

Gumbricht, T., McCarthy, T.S., McCarthy, J., Roy, D.P., Frost, P.E. and Wessels, K. 2002 Remote sensing to detect sub-surface peat fires and peat fire scars in the Okavango Delta, Botswana. South African Journal of Science 98(7 and 8): 351-358.

Healey, S.P., Cohen, W.B., Zhiqiang, Y. and Krankina, O.N. 2005 Comparison of tasseled cap-based Landsat data structures for use in forest disturbance detection. Remote Sensing of Environment 97(3): 301–310.

Hewlett, J.D. and Hibbert, A.R. 1967 Factors affecting the response of small watersheds to precipitation in humid areas. *In*: Sopper, H.W. and Lull, W.E. (eds.) Forest Hydrology, 275–290. Pergamon Press, New York.

Hijmans, R.J., Cameron, S.E., Parra, J.L., Jones, P.G. and Jarvis, A. 2005 Very high resolution interpolated climate surfaces for global land areas. International Journal of Climatology 25(15): 1965-1978.

Hjerdt, K.N. 2004 A new topographic index to quantify downslope controls on local drainage. Water Resources Research 40(5): 1-6.

Hoekman, D. 2007 Monitoring tropical peat swamp deforestation and hydrological dynamics by ASAR and PALSAR. IEEE Transactions on Geoscience and Remote Sensing 257–275.

Hoyt, A., Cobb, A. and Harvey, C. 2012 Applications of classical models to tropical peat. *In*: Magnusson, T. (ed.) 14th International Peat Congress, 1–8. International Peat Society, Stockholm.

Huete, A. 1988 Soil-adjusted vegetation index (SAVI). Remote Sensing of Environment 25(3): 295-309.

Ji, L., Zhang, L. and Wylie, B. 2009 Analysis of dynamic thresholds for the normalized difference water index. Photogrammetric Engineering & Remote Sensing 75(11): 1307-1317.

Joosten, H. and Clarke, D. 2002 Wise use of mires and peatlands. (p. 304). International Mire Conservation Group/International Peat Society, Greifswald, Germany.

Kaptué Tchuenté, A.T., Roujean, J-L. and De Jong, S.M. 2011 Comparison and relative quality assessment of the GLC2000, GLOBCOVER, MODIS and ECOCLIMAP land cover data sets

at the African continental scale. International Journal of Applied Earth Observation and Geoinformation 13(2): 207-219. http://www.sciencedirect.com/science/article/pii/S0303243410001352.

Kauth, R.J. and Thomas, G.S. 1976 The tasseled cap - a graphic description of the spectral-temporal development of agricultural crops as seen by Landsat. *In*: Proceedings of the Symposium on Machine Processing of Remotely Sensed Data. 4B41–4B51. LARS, Purdue University, West Lafayette, IN.

Lacaux, J.P., Tourre, Y.M., Vignolles, C., Ndione, J.A. and Lafaye, M. 2007 Classification of ponds from high-spatial resolution remote sensing: application to Rift Valley Fever epidemics in Senegal. Remote Sensing of Environment 106(1): 66-74. http://www.sciencedirect.com/science/article/pii/S0034425706002811.

Landmann, T., Schramm, M., Colditz, R.R., Dietz, A. and Dech, S. 2010 Wide area wetland mapping in semi-arid Africa using 250-meter MODIS metrics and topographic variables. Remote Sensing 2(7): 1751-1766.

Lobser, S.E. and Cohen, W. 2007 MODIS tasselled cap: land cover characteristics expressed through transformed MODIS data. International Journal of Remote Sensing 28(21-22): 5079-5101.

Lähteenoja, O., Reátegui, Y.R., Räsänen, M., Torres, D.D.C., Oinonen, M. and Page, S. 2012 The large Amazonian peatland carbon sink in the subsiding Pastaza-Marañón foreland basin, Peru. Global Change Biology 18(1): 164-178.

Maki, M., Ishiahra, M. and Tamura, M. 2004 Estimation of leaf water status to monitor the risk of forest fires by using remotely sensed data. Remote Sensing of Environment 90(4): 441-450. http://www.sciencedirect.com/science/article/pii/S0034425704000550.

McCarthy, J., Gumbricht, T. and McCarthy, T.S. 2005 Ecoregion classification in the Okavango Delta, Botswana from multitemporal remote sensing. International Journal of Remote Sensing 26(19): 4339-4357.

McCarthy, J.M., Gumbricht, T., McCarthy, T., Frost, P., Wessels, K. and Seidel, F. 2003 Flooding patterns of the Okavango wetland in Botswana between 1972 and 2000. AMBIO 32(7): 453-457.

McFeeters, S.K. 1996 The use of the normalized difference water index (NDWI) in the delineation of open water features. International Journal of Remote Sensing 17(7): 1425-1432.

Merot, P., Squividant, H., Aurousseau, P., Hefting, M., Burt, T., Maitre, V., Kruk, M., Butturini, A., Thenail, C. and Viaud, V. 2003 Testing a climato-topographic index for predicting wetlands distribution along an European climate gradient. Ecological Modelling 163(1-2): 51-71.

Montanarella, L., Jones, R.J.A. and Hiederer, R. 2006 The distribution of peatland in Europe. Mires and Peat 1: 1-10.

New, M., Lister, D., Hulme, M. and Makin, I. 2002 A high-resolution data set of surface climate over global land areas. Climate Research 21: 1–25.

Niasse, M., Afouda, A. and Amani, A. (eds.). 2004 Reducing West Africa's vulnerability to climate impacts on water resources, wetlands and desertification. IUCN, Gland, Switzerland. p. 19.

Nugroho, K., Wiradisastra, U.S., Arsyd, S., Pawitan, H. and Sudarsono. 2007 Detecting tidal flood pattern with Landsat TM remote sensing data in south Sumatra coastal area. Journal Tanah Dan Iklim 25: 27-36.

Page, S.E., Rieley, J.O. and Banks, C.J. 2011 Global and regional importance of the tropical peatland carbon pool. Global Change Biology 17(2): 798-818.

Price, J.S. 1992 Blanket bog in Newfoundland. Part 1. The occurrence and accumulation of fog-water deposits. Journal of Hydrology 135(1-4): 87-101. http://www.sciencedirect.com/science/article/pii/0022169492900827.

Quinn, P.F. and Beven, K.J. 1993 Spatial and temporal predictions of soil moisture dynamics, runoff, variable source areas and evapotranspiration for Plynlimon, mid-Wales. Hydrological Processes 7(4): 425-448.

Quinn, P.F., Beven, K.J. and Lamb, R. 1995 The ln (a/tan/β) index: how to calculate it and how to use it within the topmodel framework. Hydrological Processes 9(2): 161-182.

Quinn, P., Beven, K., Chevallier, P. and Planchon, O. 1991 The prediction of hillslope flow paths for distributed hydrological modelling using digital terrain models. Hydrological Processes 5(1): 59-79.Raisz, E. 1952. Landform Map of North Africa. Environmental Protection Branch, Office of the Quartermaster General.

Richardson, A.J. and Wiegand, C.L. 1977 Distinguishing vegetation from soil background information. Photogrammetric Engineering and Remote Sensing 43: 1541-1552.

Rodhe, A. and Seibert, J. 1999 Wetland occurrence in relation to topography: a test of topographic

indices as moisture indicators. Agricultural and Forest Meteorology 98-99: 325-340.

Rogers, A.S. and Kearney, M.S. 2004 Reducing signature variability in unmixing coastal marsh thematic mapper scenes using spectral indices. International Journal of Remote Sensing 25(12): 23172335.

Rondeaux, G., Steven, M. and Baret, F. 1996 Optimization of soil-adjusted vegetation indices. Remote Sensing of Environment 55(2): 95-107. http://www.sciencedirect.com/science/article/pii/0034425795001867.

Sheng, L., Huang, J. and Tang, X. 2011 A tasseled cap transformation for CBERS-02B CCD data. Journal of Zhejiang University - Science B 12(9): 780-786.

Short, N.M. and Blair, R.W. (eds.). 1986 Geomorphology from space. Scientific and Technical Information Branch, NASA, Washington, DC.

Skakun, R.S., Wulder, M.A. and Franklin, S.E. 2003 Sensitivity of the thematic mapper enhanced wetness difference index to detect mountain pine beetle red-attack damage. Remote Sensing of Environment 86(4): 433-443. http://www.sciencedirect.com/science/article/pii/S0034425703001123.

Trettin, C.C. 2012 Ecological characterization of peatlands in the Maloti Mountains, Lesotho. *In*: Magnusson, T. (ed.) 14th International Peat Congress. International Peat Society, Stockholm.

Wang, Y., Davis, F.W., Melack, J.M., Kasischke, E.S. and Christensen, N.L. 1995 The effects of changes in forest biomass on radar backscatter from tree canopies. Int*ernational Journal of Remote Sensing* 16(3): 503-513.

Weiss, A.D. 2001 Topographic positions and landforms analysis. Poster presentation, ESRI International User Conference, 9-13 July 2001. San Diego, CA.

Wolock, D.M. and McCabe Jr., G.J. 1995 Comparison of single and multiple flow direction algorithms for computing topographic parameters in TOPMODEL. Water Resources Research 31(5): 1315-1324.

Wood, J. 1996 The geomorphological characterisation of digital elevation models. Ph.D. Thesis University of Leicester, Leicester. http://www.soi.city.ac.uk/~jwo/phd/.

Wu, C., Munger, J.W., Niu, Z. and Kuang, D. 2010 Comparison of multiple models for estimating gross primary production using MODIS and eddy covariance data in Harvard Forest. Remote Sensing of Environment 114(12): 2925-2939.

Xiao, X., Boles, S., Frolking, S., Salas, W., Moore, B., Li, C., He, L. and Zhao, R. 2002 Observation of flooding and rice transplanting of paddy rice fields at the site to landscape scales in China using VEGETATION sensor data. International Journal of Remote Sensing 23(15): 3009-3022.

Xu, H. 2006 Modification of normalised difference water index (NDWI) to enhance open water features in remotely sensed imagery. International Journal of Remote Sensing 27(14): 3025-3033.

Yarbrough, L.D., Easson, G. and Kuszmaul, J.S. 2005 Quickbird 2 tasseled cap transform coefficients: a comparison of derivation methods. Pecora 16 Global Priorities in Land Remote Sensing, 23-27 October 2005. Sioux Falls, SD.

Yuhas, R.H., Goetz, A.F.H., and Boardman, J.W, 1992 Discrimination among semi-arid landscape end-members using the spectral angle mapper (SAM) algorithm. *In:* Green, R.O. (ed.) Summaries of the Third Annual JPL Airborne Geoscience Workshop, 147-149, NASA Jet Propulsion Laboratory Publication 92-14, vol. 1, Washington, DC.

***CIFOR Working Papers* contain preliminary or advance research results, significant to tropical forest issues, that need to be published in a timely manner. They are produced to inform and promote discussion. Their content has been internally reviewed but has not undergone the lengthier process of external peer review.**

The extent, volume and carbon content of the world's tropical wetlands are not accurately known. Present estimates are based on disparate sources, of varying quality from different regions. As wetlands are key regulators not only of the global carbon cycle, but also other biogeochemical cycles, better maps of wetlands are urgently needed. This report presents a set of novel approaches for mapping global tropical wetlands from a variety of image data obtained from satellite images of earth.

- Wetlands only occur under certain topographic positions, and where the climate system provides sufficient water. Combining a global digital elevation model with global climate data, a tropical global map of topographic wetness was created.
- Using global optical satellite images from a moderate resolution imaging spectroradiometer (MODIS) a second wetness index was developed. In contrast to previous satellite-based wetness indexes, the index attempts to remove the vegetation influence and focus on the soil surface wetness. From an annual time-series of MODIS images, the inundation cycle of the global tropics was captured.
- As wetlands are characterised by annual variations in inundation, an approach for classifying wetlands from a chrono-sequence of annual MODIS images was developed. In the chrono-sequence, only locations with similar climatic seasonality, and within spatial proximity are classified based on any reference site.

The wetness indexes and the chrono-sequence classification scheme are strong candidates for mapping the distribution of global tropical wetlands.

This research was carried out by CIFOR as part of the CGIAR Research Programme, 'Forests, Trees and Agroforestry: Livelihoods, Landscapes and Governance'. The Programme aims to enhance management and use of forests, agroforestry and tree genetic resources across the landscape from forests to farms. CIFOR leads the collaborative Programme in partnership with Bioversity International, the International Center for Tropical Agriculture and the World Agroforestry Centre.

cifor.org

blog.cifor.org

USAID FROM THE AMERICAN PEOPLE

FOREST SERVICE US DEPARTMENT OF AGRICULTURE

CIFOR

Center for International Forestry Research

CIFOR advances human wellbeing, environmental conservation and equity by conducting research to inform policies and practices that affect forests in developing countries. CIFOR is one of 15 centres within the Consultative Group on International Agricultural Research (CGIAR). CIFOR's headquarters are in Bogor, Indonesia. It also has offices in Asia, Africa and South America.

CGIAR